

RESEARCH ARTICLE

10.1002/2016JD024796

Key Points:

- Ten-year regional climate simulations at convection-permitting 4 km and convection-parameterizing 25 km grid spacings are performed
- The 4 km simulation better reproduced the magnitude of extreme precipitation, the diurnal cycle of precipitation, and the Great Plains LLJ
- Both simulations have similar precipitation low bias over the Great Plains and high bias over the Rockies consistent with circulation bias

Correspondence to:

M. Xue,
mxue@ou.edu

Citation:

Sun, X., M. Xue, J. Brotzge, R. A. McPherson, X.-M. Hu, and X.-Q. Yang (2016), An evaluation of dynamical downscaling of Central Plains summer precipitation using a WRF-based regional climate model at a convection-permitting 4 km resolution, *J. Geophys. Res. Atmos.*, 121, 13,801–13,825, doi:10.1002/2016JD024796.

Received 16 JAN 2016

Accepted 5 NOV 2016

Accepted article online 9 NOV 2016

Published online 2 DEC 2016

An evaluation of dynamical downscaling of Central Plains summer precipitation using a WRF-based regional climate model at a convection-permitting 4 km resolution

Xuguang Sun^{1,2}, Ming Xue^{1,2}, Jerald Brotzge^{2,3}, Renee A. McPherson⁴, Xiao-Ming Hu², and Xiu-Qun Yang¹

¹School of Atmospheric Sciences, Nanjing University, Nanjing, China, ²Center for Analysis and Prediction of Storms, University of Oklahoma, Norman, Oklahoma, USA, ³New York State Mesonet, University at Albany-SUNY, Albany, New York, USA, ⁴South Central Climate Science Center, University of Oklahoma, Norman, Oklahoma, USA

Abstract A significant challenge with dynamical downscaling of climate simulations is the ability to accurately represent convection and precipitation. The use of convection-permitting resolutions avoids cumulus parameterization, which is known to be a large source of uncertainty. A regional climate model (RCM) based on the Weather Research and Forecasting model is configured with a 4 km grid spacing and applied to the U.S. Great Plains, a region characterized by many forms of weather and climate extremes. The 4 km RCM is evaluated by running it in a hindcast mode over the central U.S. region for a 10 year period, forced at the boundary by the 32 km North America Regional Reanalysis. The model is also run at a 25 km grid spacing, but with cumulus parameterization turned on for comparison. The 4 km run more successfully reproduces certain observed features of the Great Plains May-through-August precipitation. In particular, the magnitude of extreme precipitation and the diurnal cycle of precipitation over the Great Plains are better simulated. The 4 km run more realistically simulates the low-level jet and related atmospheric circulations that transport and redistribute moisture from Gulf of Mexico. The convection-permitting RCM may therefore produce better dynamical downscaling of future climate when nested within global model climate projections, especially for extreme precipitation magnitudes. The 4 km and 25 km simulations do share similar precipitation biases, including low biases over the central Great Plains and high biases over the Rockies. These biases appear linked to circulation biases in the simulations, but determining of the exact causes will require extensive, separate studies.

1. Introduction

Dynamical downscaling of global climate model output by a high-resolution regional climate model (RCM), a technique pioneered by Dickinson *et al.* [1989] and Giorgi and Bates [1989], is now a commonly accepted method for improving the accuracy and precision of coarser-resolution climate projections. Taking advantage of the increase in horizontal grid resolution made possible by RCMs is a proven and effective way for better capturing the spatial and temporal characteristics of precipitation, extreme precipitation events, and the diurnal cycle of precipitation [Mass *et al.*, 2002; Pope and Stratton, 2002; Roeckner *et al.*, 2006; Salathé *et al.*, 2008; Shaffrey *et al.*, 2009; Borberg *et al.*, 2010; Rauscher *et al.*, 2010; Kopparla *et al.*, 2013; Prein *et al.*, 2013]. Run at higher resolutions, RCMs can better represent the topography and land surface processes with more realistic model dynamics than coarser models as well [Kopparla *et al.*, 2013; Prein *et al.*, 2013]. RCMs are highly sensitive to land surface physics and associated parameterization schemes [Bukovsky and Karoly, 2009; Hohenegger *et al.*, 2009], and high-resolution downscaling is expected to have large impacts on simulating precipitation and surface hydrology in regions with complex orography [e.g., Leung *et al.*, 2004; Qian *et al.*, 2010].

Almost all existing RCM downscaling studies use grid spacings of 10 km or larger. Such models require the use of cumulus parameterization, which is known to be one of the largest sources of uncertainty for precipitation forecasting [e.g., Molinari and Dudek, 1992; Weisman *et al.*, 1997; Dai *et al.*, 1999; Brockhaus *et al.*, 2008]. When the horizontal grid spacing is 4 km or less [Weisman *et al.*, 1997], it becomes possible to explicitly depict larger convective circulations. Such high-resolution RCMs can be called “convection-permitting (CP)” or “convection-resolving” RCMs, depending on the actual resolution used, and they are expected to have higher

prediction skill than coarser-resolution RCMs. CP models have already been regularly used in numerical weather prediction and research simulations focusing on precipitation and severe weather forecasting [e.g., *Mass et al.*, 2002; *Roberts and Lean*, 2008; *Xue et al.*, 2007, 2008, 2009, 2011, 2013; *Schwartz et al.*, 2009; *Kong et al.*, 2011]. For example, over the past decade, experimental real-time ensemble forecasts, run at convective-permitting resolutions (3 to 4 km grid spacing) over the continental U.S., have been carried out at the University of Oklahoma as part of the NOAA Hazardous Weather Testbed program [*Xue et al.*, 2007, 2008, 2009, 2011; *Kong et al.*, 2011; *Clark et al.*, 2012].

Relatively few studies have applied CP resolutions to climate simulations, largely because of the high computational cost for long-term integrations. With a monthlong CP simulation over the Alpine region, *Hohenegger et al.* [2008] found that precipitation maxima were better localized, a cold bias was reduced, and the timing of summertime precipitation diurnal cycle was improved compared to its driving lower resolution integration. *Trapp et al.* [2011] carried out individual 24-hour-long integrations during April–June for 10 years with a 4.25 km grid spacing over a large portion of the conterminous United States and showed that despite positive biases, the CP simulations yielded precipitation with diurnal cycle and geographic distributions that were consistent with observations. Targeting the eastern U.S., *Gao et al.* [2012] ran Weather Research and Forecasting (WRF) at a 4 km grid spacing forced by a coupled global climate model (CGCM) for two 4 year periods and demonstrated statistically significant improvement over the CGCM in reproducing observed extreme weather events. Focusing on the European Alps, *Prein et al.* [2013] compared results of climate simulations at a 3 km grid spacing with their 10 km parent simulations and found that 3 km simulation improved the diurnal cycle of summer precipitation, the intensity of extreme precipitation events, and the size and shape of precipitation objects. *Mahoney et al.* [2013] downscaled WRF to the storm scale (1.3 km grid spacing) for 10 extreme precipitation events selected from the 50 km grid spacing North American Regional Climate Change Assessment Program (NARCCAP) [*Mearns et al.*, 2009, 2012] simulations. A comparison of the RCM simulations revealed that the very high-resolution dynamical downscaling enabled a more detailed representation of extreme precipitation events and their relationship to their surrounding environments with less parameterization-based uncertainty.

While some of the previous CP climate simulations focused on the western U.S. where complex orography dominates [e.g., *Pan et al.*, 2011; *Mahoney et al.*, 2013] or the eastern U.S. [e.g., *Gao et al.*, 2012], only a few studies have paid attention to the Central Great Plains [e.g., *Lee et al.*, 2007; *Trapp et al.*, 2011]. The U.S. Great Plains region, defined as the area between the Rocky Mountains and Mississippi River, from Texas north to North Dakota, represents a dramatic transition in eco-climate system diversity and occurrence of extreme events [*Garbrecht and Rossel*, 2002; *Garbrecht et al.*, 2004]. The frequency and intensity of heavy precipitation events across this area have been increasing and are projected to continue to increase in the future [e.g., *Karl and Knight*, 1998; *Kunkel et al.*, 1999; *Groisman et al.*, 2001, 2004, 2005, 2012; *Higgins et al.*, 2011; *Gao et al.*, 2012; *Villarini et al.*, 2013]. The regional hydroclimate is particularly sensitive to land surface moisture and springtime convection and is strongly dependent on moisture transport from the Gulf of Mexico via the Great Plains low-level jet (LLJ) [e.g., *Bonner*, 1968; *Rasmusson*, 1967; *Higgins et al.*, 1997, 2011; *Dirmeyer and Brubaker*, 1999; *Ruiz-Barradas and Nigam*, 2005, 2006; *Cook et al.*, 2008; *Weaver and Nigam*, 2008]. The intensity of the summer mean LLJ is tightly related to the occurrence and intensity of droughts and floods [*Higgins et al.*, 1997, 2011; *Dirmeyer and Brubaker*, 1999; *Moore et al.*, 2012]. Flooding often occurs downstream of the LLJ wind maximum in the region of strongest low-level convergence [*Means*, 1956; *Maddox et al.*, 1979].

The diurnal cycle of precipitation is another unique feature of the Great Plains climate, with the rainfall reaching a maximum diurnal peak overnight during the summer months [e.g., *Wallace*, 1975; *Carbone et al.*, 2002; *Carbone and Tuttle*, 2008; *Surcel et al.*, 2010; *Berenguer et al.*, 2012]. Its nocturnal precipitation peak comes from three primary sources: eastward propagation of storms initiated over the Rocky Mountains in the late afternoon [*Carbone et al.*, 2002; *Jiang et al.*, 2006; *Carbone and Tuttle*, 2008; *Chen et al.*, 2009], a mountain-plain solenoid circulation that suppresses day-time convection and promotes nocturnal convection east of the Rocky Mountains [*Dai et al.*, 1999; *Carbone and Tuttle*, 2008], and transportation of energetic air into the Plains by the nocturnal LLJ [*Higgins et al.*, 1997; *Carbone and Tuttle*, 2008; *Pu and Dickinson*, 2014]. Simulation of this diurnal cycle is expected to be significantly improved through increasing horizontal resolution [*Lee et al.*, 2007; *Clark et al.*, 2007, 2009; *Hohenegger et al.*, 2008], especially with the use of CP modeling to explicitly represent convection [*Clark et al.*, 2007, 2009]. Simulation of the diurnal cycle is also a valuable aspect of model skill verification [*Dai et al.*, 1999; *Lin et al.*, 2000; *Trenberth et al.*, 2003; *Dai and Trenberth*, 2004].

In partnership with the South Central Climate Science Center, the Center for Analysis and Prediction of Storms is developing a CP RCM aiming at improving the dynamical downscaling of convective precipitation. The WRF model has been found to be able to produce precipitation that is more realistic than that from its driving systems [Bukovsky and Karoly, 2011; Bukovsky et al., 2013]. In this study, WRF version 3.5.1 [Skamarock et al., 2008] is coupled with the Community Land Model version 4 (CLM4) [Oleson et al., 2010; Lawrence et al., 2011] and is run at a 4 km grid spacing across a domain that includes most of the Central Great Plains. For comparison purposes, the same WRF model is also run at a 25 km grid spacing but with the inclusion of cumulus parameterization. The 4 km and 25 km simulations are run in a hindcast mode for a 10 year period from 1999 to 2009, initialized and forced at the lateral boundary by using the 32 km National Centers for Environmental Prediction (NCEP) North American Regional Reanalysis (NARR) [Mesinger et al., 2006]. Model outputs are compared against observations of May–August (May, June, July, and August or MJJA) precipitation across the domain, with particular emphasis on rainfall spatial distribution and amount, rainfall diurnal cycle, and associated atmospheric circulations such as the LLJ. This study emulates the work of the NARCCAP in Phase 1 that aims to evaluate the performance of RCMs at a 50 km grid spacing driven by National Centers for Environmental Prediction–Department of Energy (NCEP–DOE) Global Reanalysis 2 over North America [Mearns et al., 2012]. The main differences are with the use of higher resolutions, the use of NARR as the driving boundary conditions, and a smaller domain over the central U.S.

The rest of this paper is organized as follows. Observational and reanalysis data are presented in section 2, and a model description and experimental design are introduced in section 3. The model results are compared against observations of MJJA precipitation in section 4. More specific comparisons of the diurnal cycle and associated atmospheric circulations are presented in section 5. A summary and discussion are given in section 6.

2. Observational and Reanalysis Data

The Stage IV precipitation and the NARR data sets are used for simulation verification. Initial and lateral boundary conditions of RCMs are also derived from the NARR. They are described below.

2.1. Stage IV Precipitation Data

The Stage IV precipitation is a near-real-time product based on the regional hourly/6-hourly multisensor (radar plus gauges) precipitation analyses and is generated at NCEP separately from the National Weather Service (NWS) Precipitation Processing System and the NWS River Forecast Center rainfall processing. These data are mosaicked into a national product of 4 km grid spacing (on a polar-stereographic grid) and are available for hourly, 6-hourly, and daily accumulation intervals [Lin and Mitchell, 2005; Prat and Nelson, 2015]. Stage IV represents the final stage of the precipitation processing, and the data have been archived continuously since January 2002, and available via <http://data.eol.ucar.edu/codiac/dss/id=21.093>. Eight years (2002–2009) of Stage IV precipitation data are used for model comparisons in this study. Stage IV displays an overall good agreement with surface observations, although it has been shown to have a tendency of underestimation for annual and seasonal means [Prat and Nelson, 2015]. Over the Rocky Mountains, it likely underestimates precipitation due to the lack of good gauge coverage and mountain blockage of radar beams.

2.2. NCEP North American Regional Reanalysis (NARR)

NARR is a high-resolution (32 km/29-layer), high-frequency (3 h intervals) atmospheric and land surface hydrological reanalysis data set available for the North American domain. The NARR substantially improves the accuracy of temperature, winds, and precipitation compared to the NCEP–DOE Global Reanalysis 2 due to improvements in the model and data assimilation and the higher spatial resolution employed [Mesinger et al., 2006]. The agreement of summer NARR precipitation with observations over land has been shown to be relatively good [Mesinger et al., 2006] due to the assimilation of precipitation data, especially over the continental United States [Bukovsky and Karoly, 2007]. However, extreme precipitation is likely underestimated given the relatively coarse, nonconvection-resolving resolution of the forecast model used, and the smoothing effect when precipitation observations are analyzed to the model grid points. NARR covers the period from January 1979 to near present. Ten years of NARR data (1 September 1999 to 31 December 2009) are used to provide the initial condition and lateral boundary forcing for our WRF RCM runs.

Table 1. Model Configurations

	WRF-LowRes	WRF-HighRes
Version	WRF v3.5.1 ARW	WRF v3.5.1 ARW
Radiation	CAM3 shortwave and longwave	CAM3 shortwave and longwave
Boundary layer	YSU	YSU
Microphysics	WSM6	WSM6
Cumulus convection	Grell-Freitas	None
Land surface model	CLM4/10-layer	CLM4/10-layer
Vegetation types	U.S. Geological Survey (USGS) 24 classes	USGS 24 classes
Vertical levels	35	35
Horizontal resolution	25 km/101 × 117	4 km/621 × 721
Sponge zone	10.5 points	10.5 points
Time step	75 s	12 s
Integration	From 1/9/1999 to 31/12/2009	From 1/9/1999 to 31/12/2009
Lateral boundary	NARR-a/32 km	NARR-a/32 km

3. Model Descriptions and Experimental Designs

WRF is a fully compressible, nonhydrostatic model with hydrostatic-pressure-based terrain-following vertical coordinates [Skamarock *et al.*, 2005]. The version 3.5.1 of WRF is used, and the model is coupled with the Community Land Model version 4 (CLM4) that was originally developed for the Community Earth System Model (<http://www2.cesm.ucar.edu/>) for Earth system and climate simulations [Oleson *et al.*, 2010; Lawrence *et al.*, 2011]. Compared to the Noah land surface model [Ek *et al.*, 2003] that is commonly used for numerical weather prediction and short-range simulations, CLM4 has more sophisticated treatments of vegetation and hydrological processes, including interactive vegetation canopy, groundwater, and multilayer snow [Cai *et al.*, 2014]. The 4 km and 25 km simulations have the same physics parameterization schemes except that cumulus parameterization is not used by the 4 km simulation. The schemes used the Community Atmosphere Model 3 (CAM3) radiation physics, Yonsei University (YSU) planetary boundary layer (PBL) scheme, and WRF 6-category single-moment microphysics (WSM6). The 25 km simulation includes in addition the newer Grell-Freitas [Grell and Freitas, 2013] cumulus parameterization scheme (see Table 1). Due to limited computational resources available, we did not test other physics combinations on the 4 km grid, although such comparisons and the sensitivity of the simulations to model physics should be investigated in the future.

The 4 km and 25 km simulations are named “WRF-HighRes” and “WRF-LowRes,” respectively, in this paper. Both simulations cover a domain encompassing much of the Central U.S. (about 20°N–50°N and 110°W–88°W) (Figures 1a and 1b) and are forced by 3-hourly NARR reanalysis and initialized at 0000 UTC on 1 September 1999, run continuously until 31 December 2009 (about 10 years). The detailed model configurations are listed in Table 1. The 4 month period from 1 September to 31 December of 1999 is considered a period of spin-up, and model output for MJJA from the 10 year period from 2000 to 2009 are used for evaluation.

To perform equitable comparisons, all precipitation and atmospheric variable fields are regridded to a common 25 km grid by using the “patch recovery” technique of the ESMF software (<https://www.earthsystemcog.org/projects/esmf>). The patch recovery technique typically results in better approximations of values and derivatives when compared to bilinear interpolation. To more quantitatively evaluate the quality of precipitation simulations, spatial pattern correlation and root-mean-square error (RMSE) of MJJA precipitation in the evaluation domain of South Central Plains are calculated for NARR, the 4 km and 25 km WRF simulations against Stage IV data (Table 2).

4. RCM Evaluation: Summer Mean Precipitation

4.1. Precipitation

Figure 2 presents 10 year mean MJJA precipitation distributions over much of the simulation domain. As seen in the Stage IV precipitation (Figure 2a), the MJJA mean precipitation is heaviest across northern and central Plains, from Oklahoma to Missouri, and along the northern coast of the Gulf of Mexico from the southeastern Texas coast onward to the east. One particular area with a precipitation maximum—northeast Oklahoma and southeast Kansas (OKKS)—is marked by a dashed rectangle in all panels of Figure 2. The NARR generally

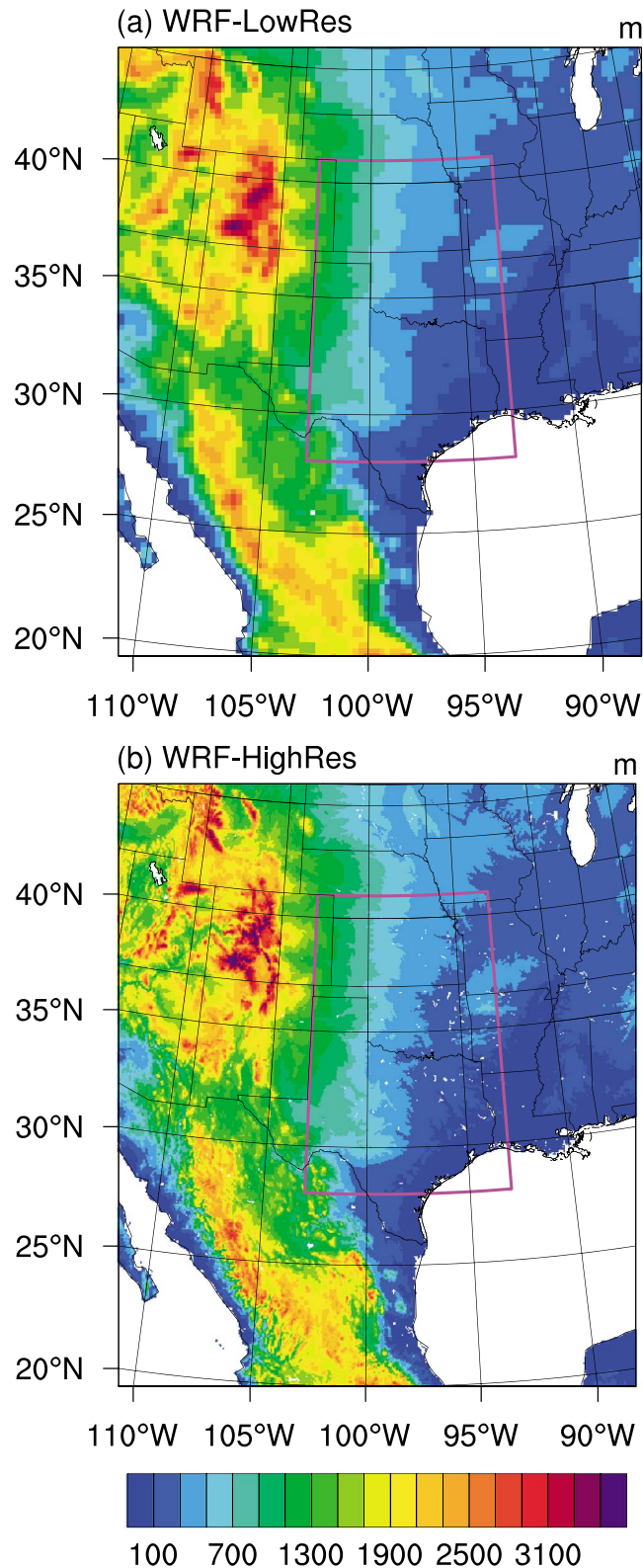


Figure 1. Topography height in model domain of (a) WRF-LowRes (25 km) and (b) WRF-HighRes (4 km); unit is in meter. The solid quadrangle encloses a central Great Plains domain for focused comparisons in this study, which is also marked in Figures 2–5.

depicts similar locations of the maxima with a pattern correlation coefficient of 0.85 over the solid quadrangle shown in Figure 1 (Figure 2b and Table 2). In our 4 km WRF run (WRF-HighRes) (Figure 2c), the lower values of MJJA precipitation in southwestern Texas are reasonably well captured. However, there is an overall positive bias across much of the domain and large positive biases over mountainous terrain and near the southern and eastern boundaries of the domain. The precipitation biases in the 25 km WRF run (WRF-LowRes) are similar in most areas but are worse than WRF-HighRes over the northwestern Gulf of Mexico (Figure 2d). Over our main evaluation domain in this paper in the South-Central Plains enclosed by the solid quadrangle in Figures 1–6, the 4 km WRF run generally reproduces the spatial distribution of MJJA rainfall of Stage IV with a pattern correlation coefficient of 0.46, which is slightly higher than that of 25 km WRF run (0.42), and the difference of the pattern correlation coefficients is significant at a 90% confidence level based on Z test. The similar and relative low pattern correlations indicate that WRF has systematic biases in simulating the distribution of MJJA rainfall on both 4 km and 25 km grid. On the other hand, the RMSE of 4 km WRF run is only half that of 25 km WRF run (Table 2), indicating improved MJJA mean rainfall at the 4 km grid spacing.

Over the full northern portion of the domain the west-to-east gradient of simulated precipitation is reversed, with too much rain over the Rocky Mountains and not enough over the Central Plains covered by the dashed box. The positive bias over the Rocky Mountains may partly be due to underestimation in Stage IV

Table 2. Pattern Correlation (R) and RMSE (E) Values of MJJA Precipitation for NARR, WRF-HighRes, and WRF-LowRes Compared to Stage IV Precipitation^a

Corr and RMSE	Total Rain		Light Rain		Heavy Rain		90th Percentile	
	R	E	R	E	R	E	R	E
NARR	0.85	0.5	0.71	15.2	0.74	14.9	0.52	11.4
WRF-HighRes	0.46	0.9	0.47	8.0	0.39	11.3	0.09	6.6
WRF-LowRes	0.42	1.8	0.38	17.1	0.38	16.9	0.36	10.7

^aThe evaluation domain is over the South Central Plains, which is enclosed by the solid purple quadrangle in Figure 1. Unit of RMSE is mm d^{-1} for total rain and 90th percentile, and % for light and heavy rain. Critical correlation coefficient at the 99% confidence is 0.06 for 1862 spatial grids based on Student's t test.

their 10 km grid-spacing simulation overestimated precipitation more than their 50 km simulation did. They suggested that the overestimation was partly due to scale-dependent deficiencies in the Kain-Fritsch cumulus parameterization scheme, which generated excessive precipitation and insufficient eastward propagation of convection. Lee *et al.* [2007] also found wet biases over the Rockies and dry biases over the Great Plains in global climate model (GCM) simulations, with stronger biases when the GCM resolution was increased from 2° to $1/2^\circ$, suggesting an increased locking of the precipitation to the high terrain. They suggested that their errors were associated with unrealistically strong coupling of the convection to the surface heating, among which the convective instability of the second kind induced by strong convection was involved. At this time, the root causes of the prevalent high-precipitation biases across the country and the commonly observed dry biases over the Great Plains are not exactly known, and there is a need for further studies on the causes of such biases. The fact that our 25 km and 4 km simulations have similar biases indicates that the problem is not due solely to the use of cumulus parameterization.

At a 4 km grid spacing, precipitation simulation is still very sensitive to microphysics parameterization [Schwartz *et al.*, 2010] because 4 km is not fine enough to resolve individual convective cells and their internal circulations, and it is known to have a tendency to overestimate precipitation [e.g., Weisman *et al.*, 2008; Schwartz *et al.*, 2010; Bryan and Morrison, 2012]. Some researchers have argued that the resolutions of $O(100\text{ m})$ are needed to properly resolve many important features of moist convection [e.g., Bryan *et al.*, 2003; Bryan and Morrison, 2012]. Clearly, $O(100\text{ m})$ resolution is too expensive for climate simulations. Developing resolution-aware microphysics and/or subgrid-scale turbulence parameterization schemes that compensate for resolution-related deficiencies to reduce the precipitation biases is a possible avenue, but it is beyond the scope of this study.

To understand the character of daily rainfall intensity produced by each analysis and model, the percentage of total precipitation produced at light rain rate (0.1 to 10 mm d^{-1}) and heavy rain rate ($\geq 25\text{ mm d}^{-1}$) for total MJJA-mean precipitation is computed at every grid point for each data set and shown in Figures 3 and 4, respectively. An examination of the Stage IV observational product shows that while light precipitation dominates over the Rocky Mountains, light rain contributes less than 20% of the rainfall total over the rest of the domain (Figure 3a). Heavy rainfall events, as estimated from Stage IV analyses (Figure 4a), account for over half of total MJJA rainfall from southwestern Oklahoma to northeastern Missouri as well as along much of the Gulf Coast. Indeed, areas of heavy rainfall dominate the regions of MJJA precipitation maxima. NARR shows similar broad patterns in the contributions of light and heavy precipitation to those of Stage IV (Figures 3b and 4b), but the percentage of light rain is generally overestimated and that of heavy rain is underestimated, which is consistent with its relatively low resolution. NARR pattern correlations of light and heavy rains are 0.71 and 0.74, respectively (Table 2).

Compared to WRF-LowRes, WRF-HighRes basically reproduces a distribution pattern of light precipitation percentage that is more consistent with Stage IV data (Figure 3c), but it does drastically underpredicts the frequency of these events in the mountainous terrain and Mexican Plateau. Although WRF-HighRes captures a higher percentage of heavy precipitation east of the Rockies, consistent with the Stage IV analyses (Figure 4c), but it overpredicts the occurrences of heavy precipitation, especially over the northern Gulf Coast and Louisiana and Mississippi. As for WRF-LowRes (Figures 3d and 4d), the relative contributions of light and heavy precipitation are reasonably simulated over the Rocky Mountains (better than WRF-HighRes) but are

precipitation [Prat and Nelson, 2015] but is more likely due to WRF model bias. Similar problems were also found in other studies, such as Done *et al.* [2004] and Mearns *et al.* [2012], at convection-permitting and nonconvection-permitting resolutions. Similarly, Tripathi and Dominguez [2013] found that the mean precipitation over the New Mexico was overestimated in their WRF-based climate simulations covering Arizona and New Mexico, and

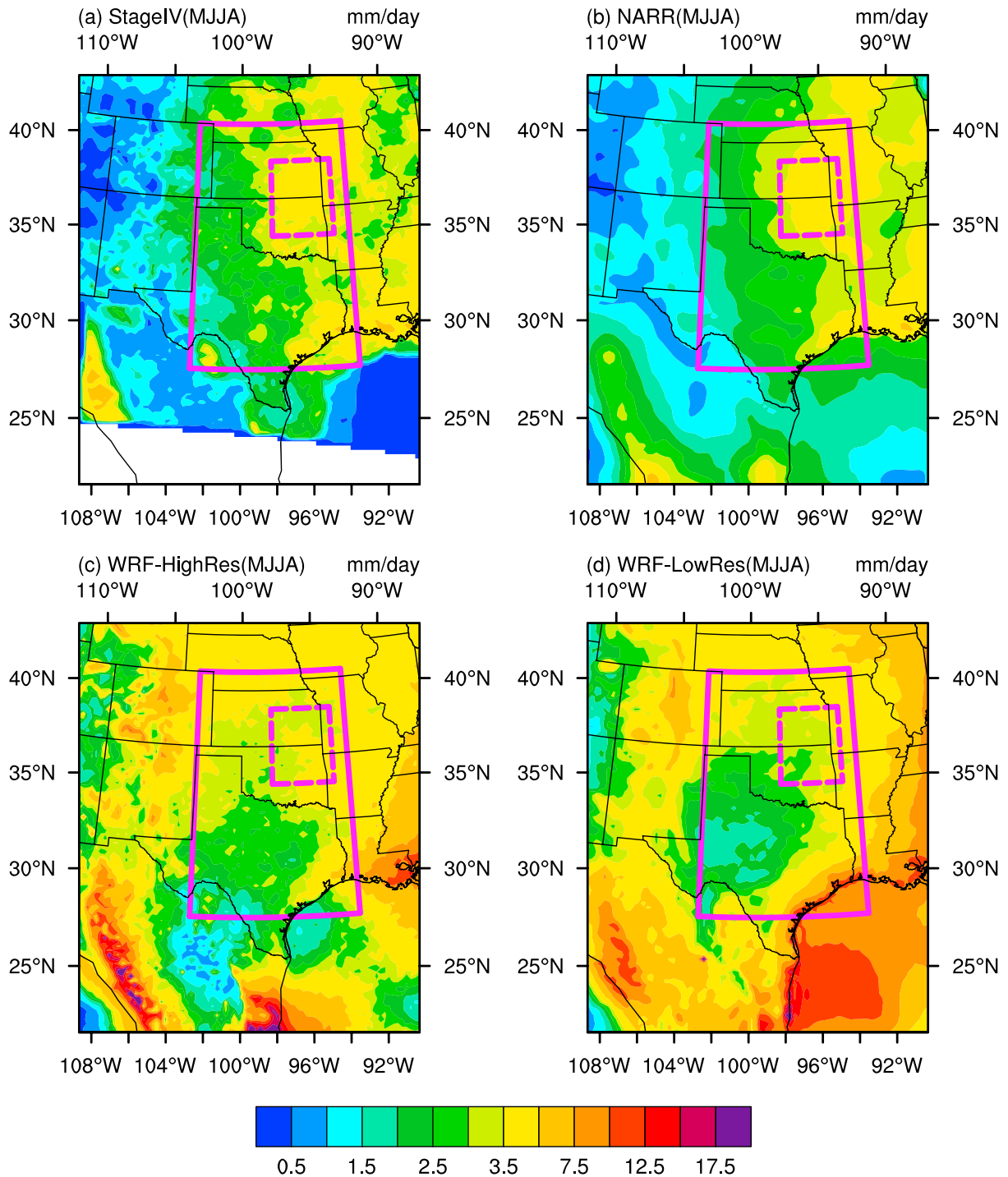


Figure 2. MJA precipitation distributions of (a) Stage IV, (b) NARR, (c) WRF-HighRes, (d) WRF-LowRes. Unit is in mm d^{-1} . The quadrangle with dashed lines indicates the Northeast Oklahoma and Southeast Kansas (OKKS) region where an observed local precipitation maximum is found. Figure 2a is the average of the 8 year (2002–2009) data. Figures 2b–2d are averages based on the 10 year (2000–2009) of data.

far from the observations (Stage IV; Figure 3a), reanalysis (NARR; Figure 3b), and WRF-HighRes (Figure 3c) over the Great Plains. In WRF-LowRes (Figure 3d), more than half of the precipitation is produced as light rain across much of Texas, a much greater percentage than in Stage IV data. As expected, WRF-LowRes (Figure 4d) has much lower contributions from heavier rainfall, with only areas in the northeastern Plains approaching 40%. Accordingly, WRF-HighRes has a higher pattern correlation with Stage IV than WRF-

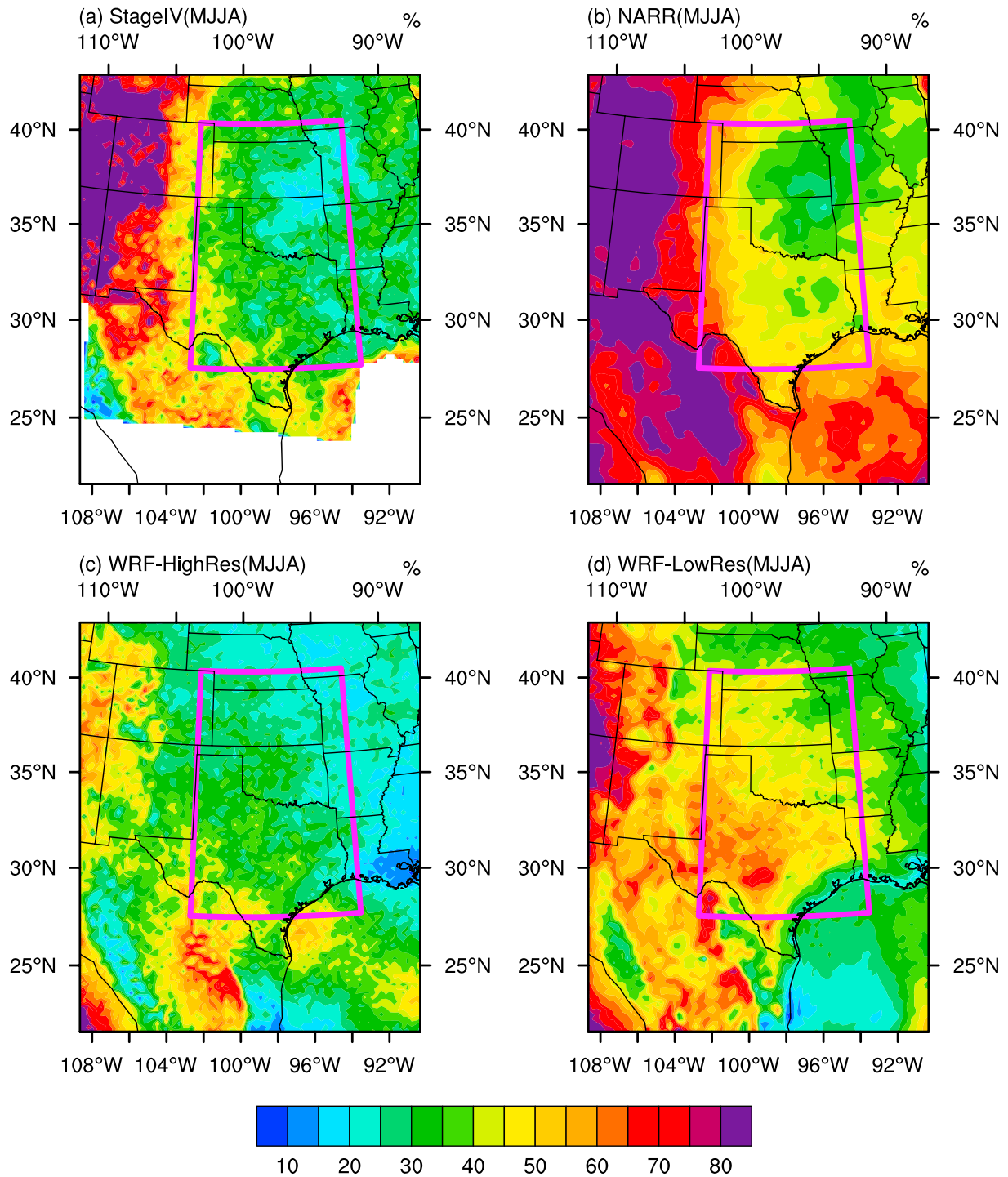


Figure 3. Percentage of total precipitation amount produced at rates between 0.1 and 10 mm d⁻¹ (for light rain) for the total amount of MJJA precipitation in (a) Stage IV, (b) NARR, (c) WRF-HighRes, and (d) WRF-LowRes (unit is %). Figure 3a is from the 8 year (2002–2009) averaged data. Figures 3b–3d are calculated based on the 10 year (2000–2009) averaged data.

LowRes for total rain (0.46 versus 0.42, significantly different at a 90% confidence level based on Z test), light rain (0.47 versus 0.38, significantly different at a 90% confidence level based on Z test), and heavy rain (0.39 versus 0.38, not statistically different at a 90% confidence level based on Z test), and its RMSE is smaller compared to WRF-LowRes (0.9 versus 1.8 for total rain; Table 2).

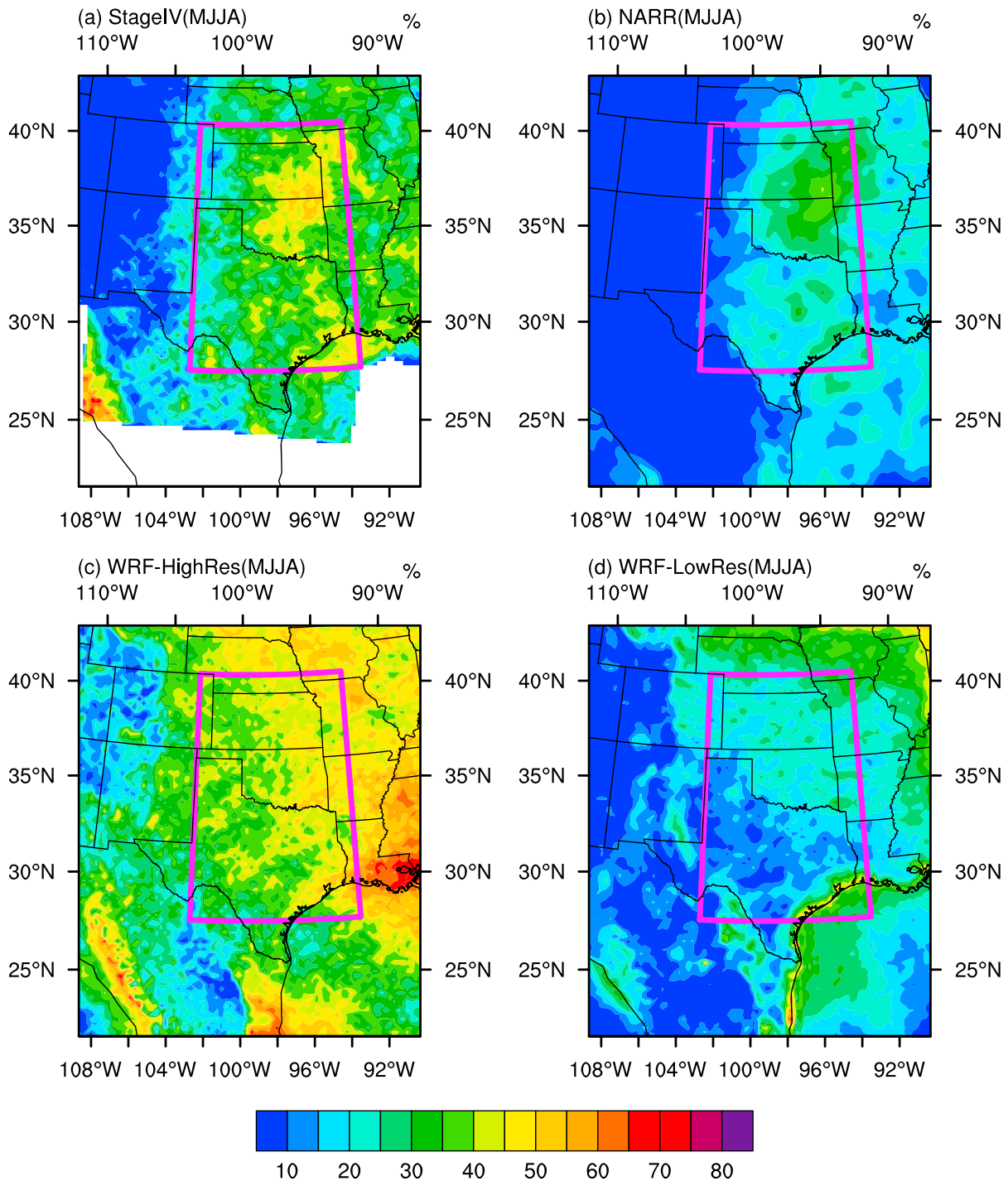


Figure 4. Same as Figure 3 but for precipitation produced at rates above 25 mm d⁻¹.

To further assess the models' abilities in reproducing observed precipitation patterns, we examine the MJJA daily precipitation events in the upper 90th percentile for different data sets. The 90th percentile is the value at 90% of the sorted precipitation data in ascending order and is often used as a threshold to define extreme precipitation. Consistent with the distribution patterns of light and heavy precipitation percentages shown in Figures 3 and 4, Stage IV data present a north-to-south swath of low values (less than 10 mm d⁻¹) over the Rocky Mountains region and a high-value center (above 40 mm d⁻¹) over the Great Plains from south-central Texas to northern Missouri (Figure 5a), which means that extreme precipitation events have greater

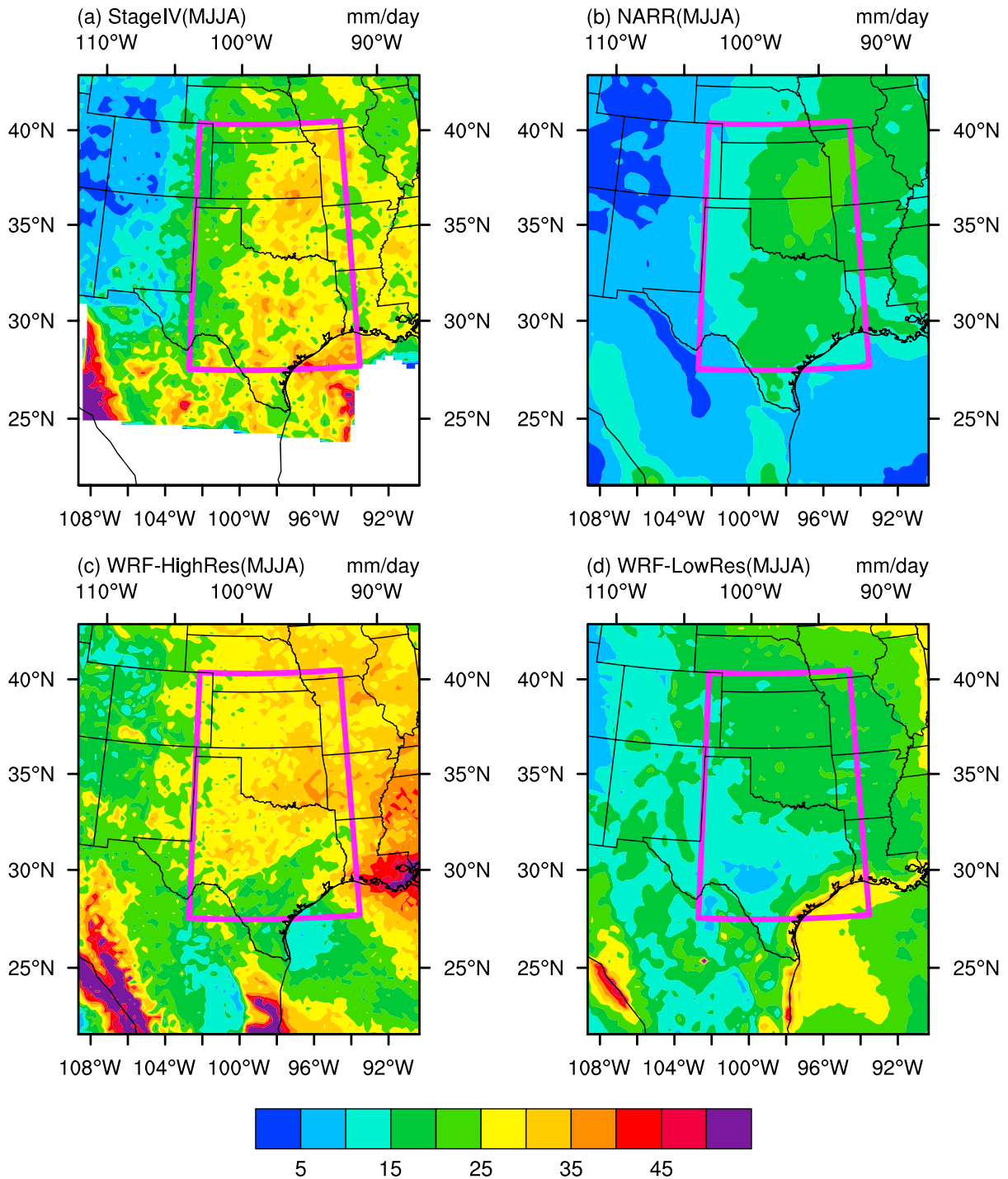


Figure 5. Values (in mm d^{-1}) for the 90th percentile of MJJA daily precipitation of (a) Stage IV, (b) NARR, (c) WRF-HighRes, and (d) WRF-LowRes. Figure 5a is from the 8 year (2002–2009) data. Figures 5b–5d are calculated based on the 10 year (2000–2009) data.

magnitudes in these Great Plains regions. NARR shows similar patterns, but its magnitude is much lower and its spatial structure is not well defined because of its lower resolutions (Figure 5b). In comparison, the WRF-HighRes RCM captures the detailed maxima over the Central Plains region (Figure 5c), but due to the reversed pattern in southern Texas, the pattern correlation over the verification region is very low (0.09). On the other hand, thanks to the well-simulated magnitude of the 90th percentile of MJJA daily precipitation, the RMSE is

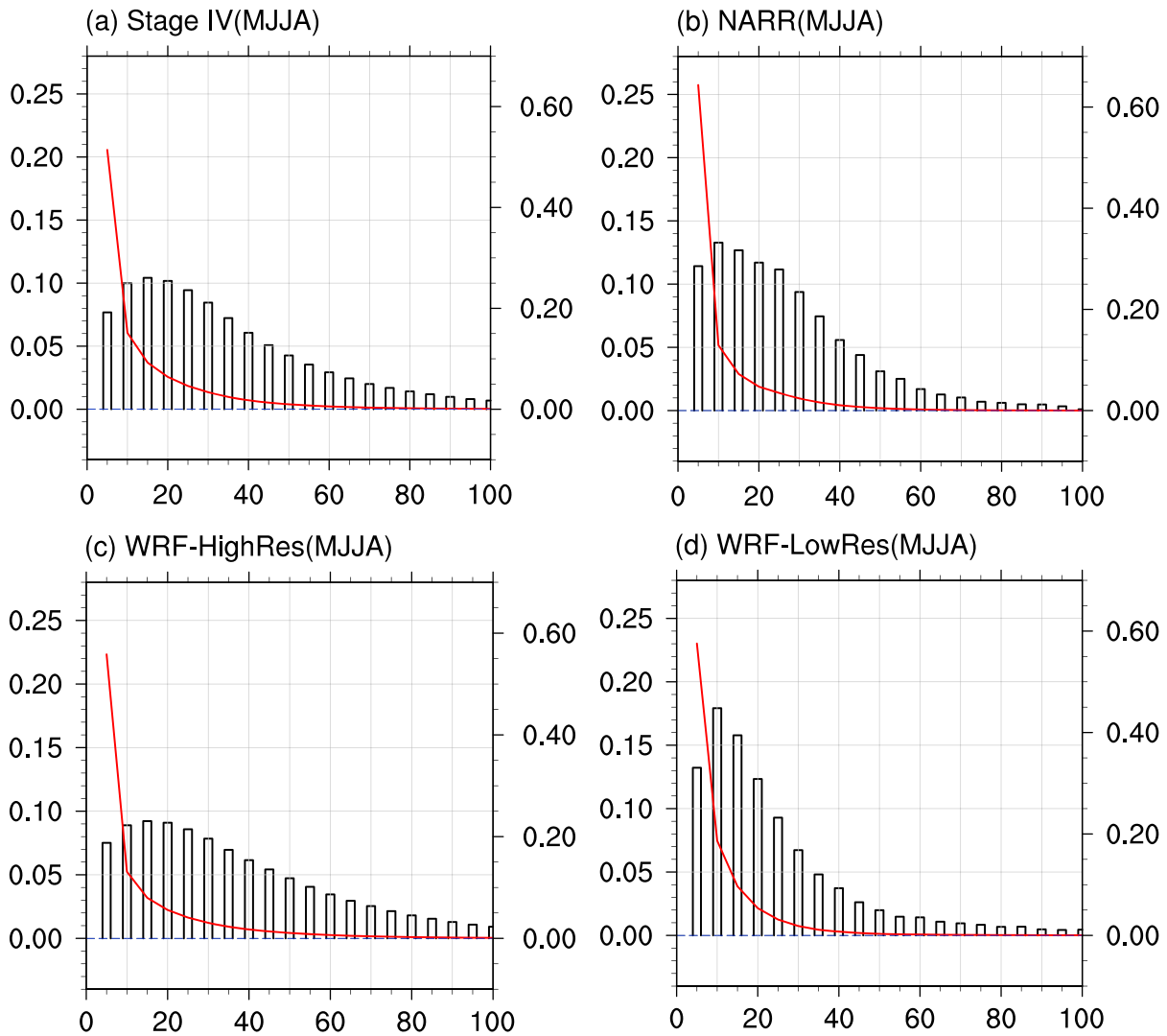


Figure 6. Probability distribution function (PDF) (red solid line, right y axis) and ratio of accumulated precipitation of every discrete interval 5 mm d^{-1} to the total MJJA precipitation amount based on MJJA daily precipitation (bar, left y axis) over the OKKS region of (a) Stage IV, (b) NARR, (c) WRF-HighRes, and (d) WRF-LowRes. Figure 6a is from the 8 year (2002–2009) data. Figures 6b–6d are calculated based on the 10 year (2000–2009) data.

only 6.6 mm d^{-1} , nearly half that of NARR (Table 2). Nevertheless, a positive bias exists over the southeastern Oklahoma and a negative bias occurs over the southern Texas (Figure 5c), which causes a very small pattern correlation with Stage IV (about 0.1; Table 2). In contrast, the WRF-LowRes RCM significantly underestimates the magnitude of the 90th percentile precipitation over much of the evaluation domain and fails to show any regional maxima across the Central Plains (Figure 5d); it has a larger RMSE (10.7 mm d^{-1}) with Stage IV, although their pattern correlation (0.36) is relatively better than the WRF-HighRes (Table 2). For extreme precipitation, the 4 km WRF-HighRes appears to provide added value in simulating the magnitude of extreme precipitation although not the spatial distribution. This confirms one advantage of CP RCMs found in previous studies for other regions and generally for shorter time periods [e.g., Hohenegger et al., 2008; Gao et al., 2012; Prein et al., 2013; Mahoney et al., 2013].

As highlighted in the dashed box in Figure 2, the Stage IV data show a regional MJJA precipitation maximum in OKKS area. To further quantify differences among the analyses and models, the probability distribution function (PDF) and binned histograms (at intervals of 5 mm d^{-1}) of the ratio of accumulated precipitation to the total MJJA amount are shown in Figure 6. As seen in Stage IV data (Figure 6a), precipitation frequencies decrease with increasing precipitation intensities, and the frequency of rainfall between 0.1 and 5 mm d^{-1} over the OKKS region accounts for half of the total precipitation frequency. As for the precipitation amount,

accumulated precipitation peaks between 10 and 15 mm d⁻¹ in the observations and accumulated precipitation above 25 mm d⁻¹ accounts for over half the total MJJA precipitation amount, consistent with Figures 4a and 5a. The WRF-HighRes RCM reproduces these MJJA daily precipitation frequencies and amounts rather well (Figure 6c). However, the reanalysis and coarse-resolution model simulation generally fail to capture these features completely (Figures 6b and 6d). For instance, in NARR (Figure 6b), the light precipitation frequency is too high, accounting for over 60% of the total precipitation frequency. On the other hand, because of the coarse grid resolution, WRF-LowRes RCM has higher frequency of light precipitation but lower frequency of heavy precipitation than analyzed by the Stage IV, data and accordingly, the contribution of extreme heavy rainfall to the MJJA precipitation total is much less than it should be (Figure 6d).

4.2. Low-Level Jet

Heavy precipitation and flooding across the U.S. Great Plains are tightly linked to the evolution of the Great Plains LLJ. The Great Plains LLJ, confined mainly within the boundary layer with maximum wind speeds typically at 500–1000 m above the ground, transports large amounts of moisture northward from the Gulf of Mexico [Higgins *et al.*, 1997; Dirmeyer and Brubaker, 1999; Dirmeyer and Kinter, 2009]. Figure 7 shows the 10 year average MJJA water vapor flux at 925 hPa. In NARR (Figure 7a), a strong subtropical high is situated off the southeast U.S., and to its west, a narrow region of strong southerly winds corresponds to the LLJ (indicated by a rectangle in Figure 7 and in Figure 1 of Jiang *et al.* [2007]). Mo *et al.* [2005] showed that the NARR's LLJ compares favorably with observations. The LLJ is depicted by WRF-HighRes well although its northern extent into Kansas is underpredicted. A local maximum of meridional moisture flux near the west coast of Gulf of Mexico is also captured. However, its southeasterly moisture flux over the Gulf of Mexico is too high (Figure 7b), which may be associated with an increase in atmospheric moisture transport from the ocean to land as its horizontal resolution increased [Demory *et al.*, 2014]. The WRF-LowRes RCM (Figure 7c) gives a broader LLJ, and its southeasterly moisture flux over the northern part of the Gulf is stronger. However, the local maximum of moisture flux over the west coast of the Gulf is mostly absent.

The difference fields between WRF-HighRes and NARR show a weaker LLJ over the Central Plains in WRF-HighRes than in NARR (Figure 7d), which appears to be linked to the underestimation of MJJA mean precipitation in the Great Plains (Figure 2c). Over the northeastern coast of the Gulf of Mexico, stronger moisture flux induces moisture convergence bias (Figure 7d) and causes excessive precipitation (Figure 2c). The weak LLJ bias in the northern Great Plains can also be seen in WRF-LowRes, but in the southern Great Plains and near the northeastern coast of Gulf of Mexico there are strong LLJ and south-southwesterly moisture flux biases (Figure 7e), contributing to large positive precipitation bias (Figure 2d). Compared to WRF-LowRes, WRF-HighRes generally has smaller positive moisture flux bias (Figure 7f), while its LLJ is weaker. These comparisons of mean circulations indicate that there are systematic circulation pattern errors or biases with the WRF RCM simulations at both 4 and 25 km resolutions, and precipitation biases can result subject to such circulation biases. Wang and Kotamarthi [2014] found that by performing spectral nudging, i.e., longer waves in the RCM solution nudged toward the external forcing, the precipitation biases were reduced. This can be a solution, although the true causes of the circulation biases should still be investigated.

To further examine the vertical structure of the LLJ and associated moisture transport, the meridional water vapor fluxes averaged over the 30°N–40°N latitudinal band are shown in Figure 8. In NARR (Figure 8a), the LLJ, depicted in terms of the maximum of the meridional moisture flux, tilts along the eastern slope of the Rocky Mountains, with its center located roughly at 925 hPa and 100°W. The WRF-HighRes RCM captures well the height and location of the LLJ, although the jet is much weaker (Figure 8b). The LLJ is stronger in the WRF-LowRes simulation; however, its center is shifted downward to about 950 hPa and eastward to about 98°W, and the tilt of the maximum axis of the flux with height is less compared to NARR (Figure 7c). The weaker intensity in the high-resolution simulation may be due to variability in the location of the LLJ. Overall, there are still significant errors in the moisture transport associated with LLJ in both 25 and 4 km simulations. It is difficult to say which one is better in this aspect.

5. Diurnal Cycle of Summer Precipitation and Associated Atmospheric Circulations

5.1. Precipitation

The anomalies of 3 h accumulated MJJA precipitation deviated from and then normalized by its daily mean are shown in Figure 9 for the Stage IV data, for 0000 through 2100 UTC at 3 h intervals. Only their positive

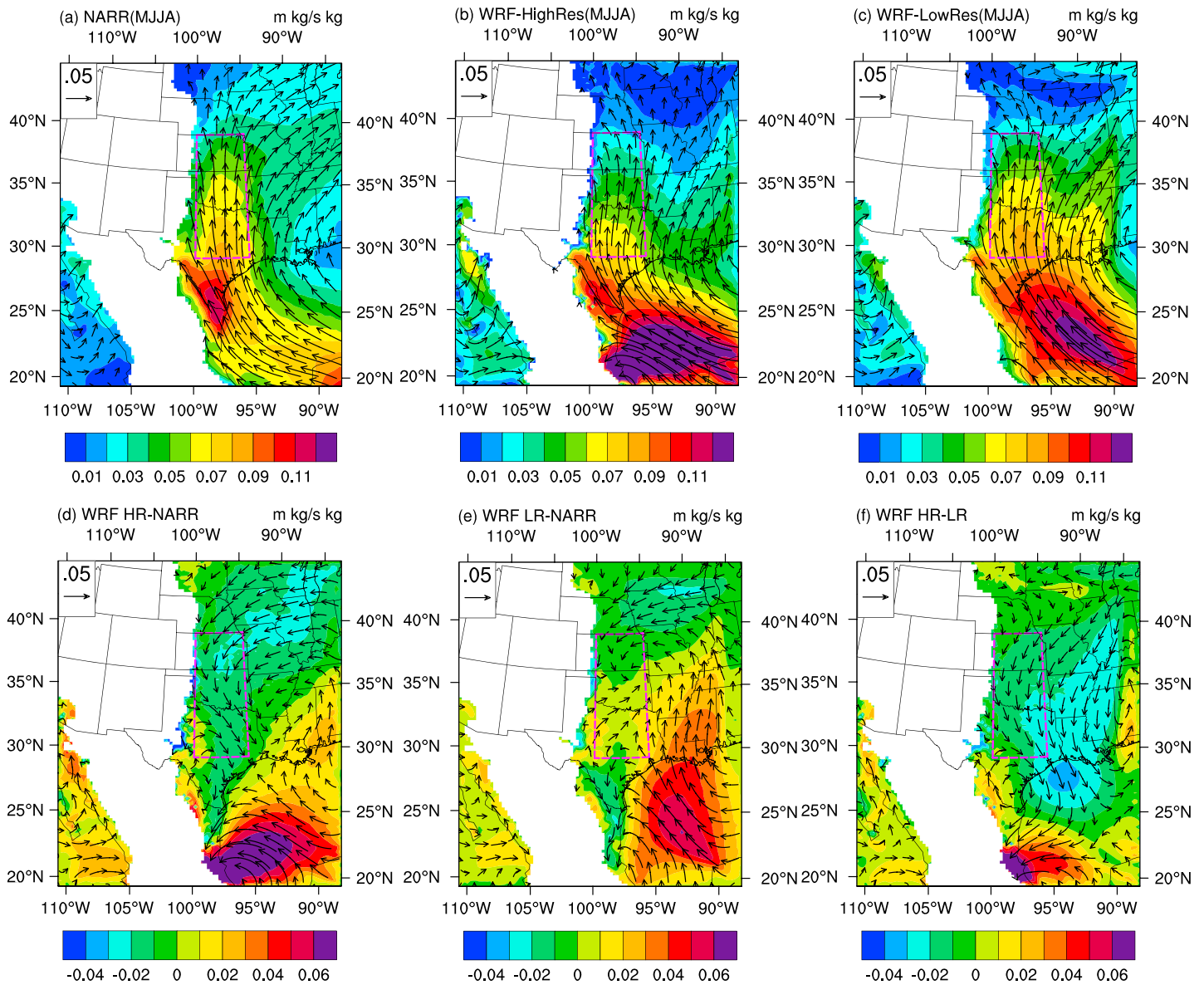


Figure 7. MJA average water vapor flux and wind vectors at 925 hPa of (a) NARR, (b) WRF-HighRes, and (c) WRF-LowRes, and the difference (d) between WRF-HighRes and NARR, (e) between WRF-LowRes and NARR, and (f) between WRF-HighRes and WRF-LowRes. Shading is the water vapor flux in $\text{m kg s}^{-1} \text{kg}^{-1}$. The rectangle box indicates the Great Plains LLJ region (100°W – 95°W , 30°N – 40°N). Regions below ground are masked out.

values are drawn because they indicate the precipitation peaks in a day. In the late afternoon (2100 to 0000 UTC), the Rocky Mountains region, with elevated heating and limited convective inhibition, is prone to precipitation. At the same time, afternoon heating combined with an ample moisture supply produces convection across the coastal and inland regions of the Gulf of Mexico (Figures 9h and 9a). During the early evening and overnight, convection over the Rockies gradually propagates eastward and decays over time (Figures 9a–9f). By early morning, this swath of precipitation reaches the Central Plains [Carbone *et al.*, 2002; Jiang *et al.*, 2006; Chen *et al.*, 2009] (Figures 9d and 9e). Generally, WRF-HighRes reproduces the diurnal cycle and propagation of MJA precipitation over the Rocky Mountains and the Great Plains well (Figure 10), except that the precipitation dissipates too fast while propagating eastward. In the early morning the precipitation maximum is found over the Central Plains, although the intensity is a little too low (Figure 10e). In comparison, the diurnal cycle and propagation of precipitation over the Great Plains region are fairly weak in WRF-LowRes (Figure 11). The early morning peak over the Central Plains is essentially absent.

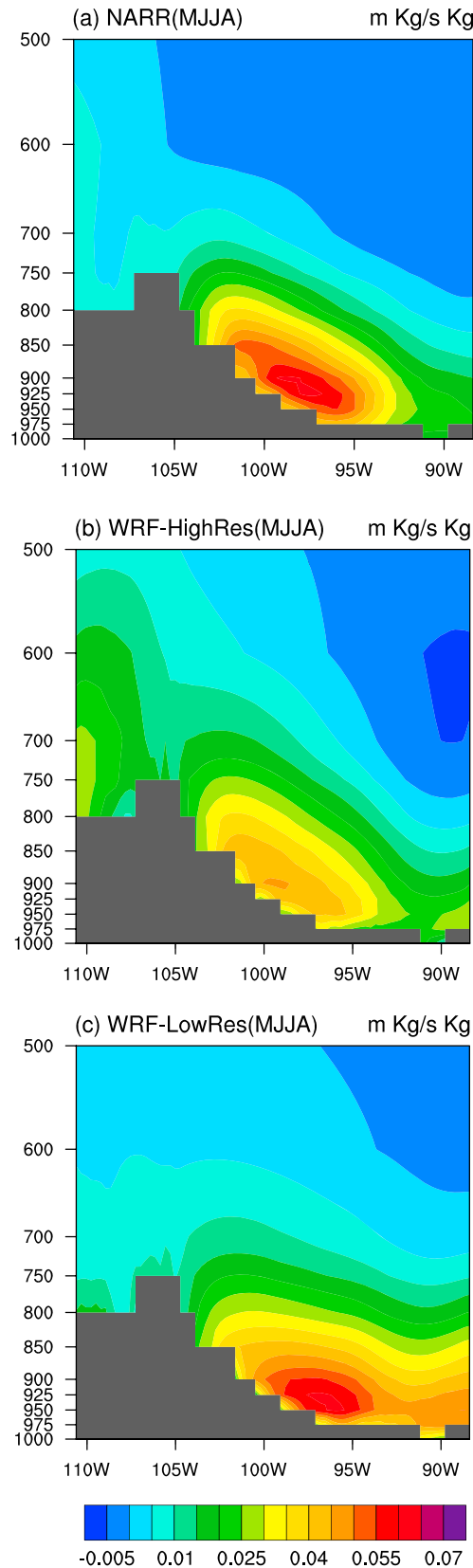


Figure 8. Meridional water vapor flux ($\text{m kg s}^{-1} \text{kg}^{-1}$) averaged over the 30–40°N latitudinal band for (a) NARR, (b) WRF-HighRes, and (c) WRF-LowRes.

To see more clearly the diurnal cycle of precipitation, Hovmöller diagrams of normalized precipitation deviations for the MJJA months, averaged between 30°N and 40°N, are shown in Figure 12. In Stage IV data (Figure 12a), afternoon precipitation is located over the Rocky Mountains (west of 150°W) and east of the Great Plains (east of 95°W). Between late afternoon and next morning, precipitation over the Rocky Mountains propagates eastward to about 95°W, where a semidiurnal precipitation signal forms [Carbone *et al.*, 2002]. The NARR analysis has a similar (albeit weaker) pattern of diurnal propagation [Jiang *et al.*, 2006] (Figure 12b). WRF-HighRes (Figure 12c) reproduces successfully the eastward propagation of precipitation generated over the Rockies. While the eastward propagating precipitation dissipates around 97°W at around 1200 UTC, the intensity of the simulated diurnal signal before 0600 UTC is comparable to that of the Stage IV analysis; afterward, it dissipates much faster. Corresponding to the general overprediction of precipitation in the eastern 1/3 of model domain as seen in Figure 5c, there is overprediction of late afternoon to early evening precipitation in the eastern part of domain in WRF-HighRes. In WRF-LowRes (Figure 12d), the diurnal rainfall maximum peaks over the entire domain in the late afternoon to early evening, and there is little eastward propagation in precipitation. Clearly, the propagation and therefore the diurnal cycle of precipitation are poorly handled in WRF-LowRes,

5.2. Zonal Circulations

To better understand the behaviors of diurnal variations of MJJA precipitation across the Rocky Mountains and Great Plains regions, east-west cross sections

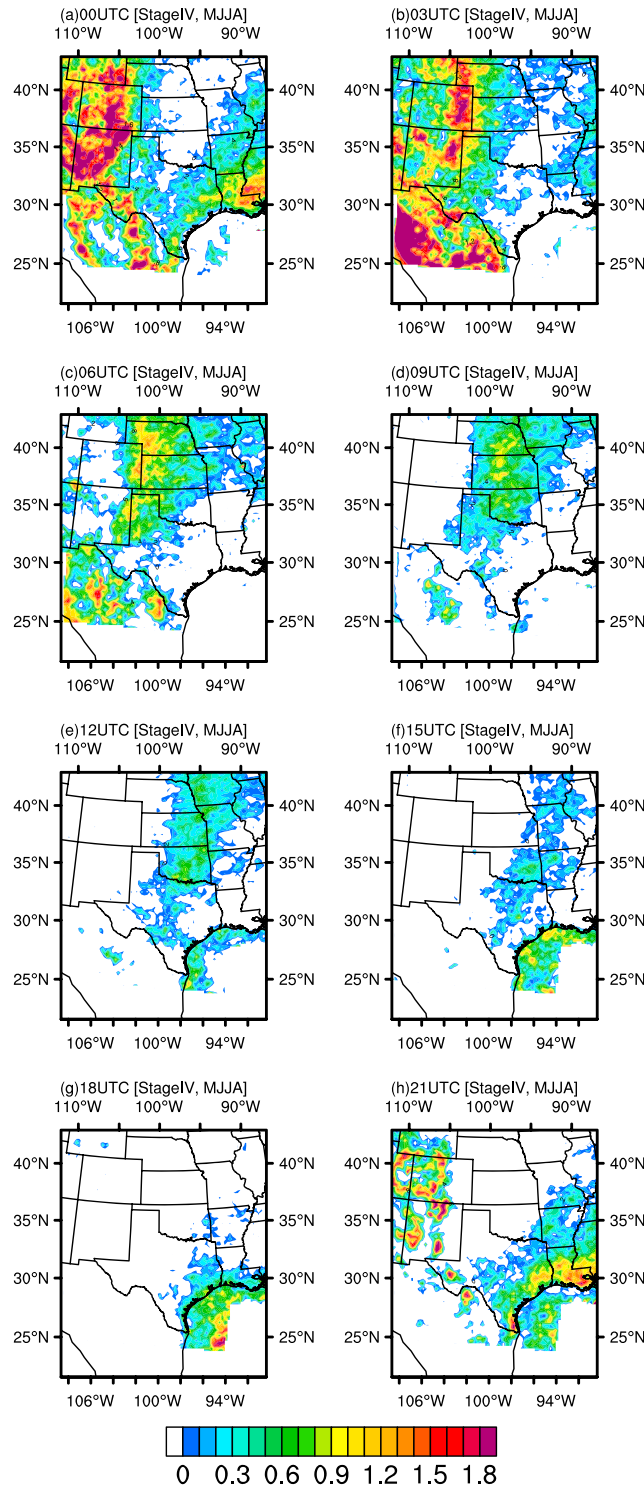


Figure 9. Normalized diurnal precipitation deviations at (a) 00:00, (b) 03:00, (c) 06:00, (d) 09:00, (e) 12:00, (f) 15:00, (g) 18:00, and (h) 21:00 UTC of the 8 year (2002–2009) average Stage IV MJJA precipitation.

of diurnal deviations (from daily mean) of zonal vertical circulation, meridional wind, and temperature averaged over 30–40°N are presented for NARR data for different times of the day in Figure 13. Over the Rocky Mountains, the boundary layer temperature peaks in the afternoon (2100 to 0000 UTC, corresponding to 1400 to 1700 local standard time) because of strong insolation (Figures 13h and 13a) and becomes a relative heat source compared to its surroundings. This induces two effects: a westward pressure gradient force east of the mountains and convergent flow toward the mountains. Correspondingly, a mountain–plain solenoid circulation forms with upward vertical motion over the Rocky Mountains and downward vertical motion over the Great Plains [Carbone and Tuttle, 2008], which favors more precipitation over the Rocky Mountain regions but suppresses rainfall over the Plains regions in the afternoon (Figures 9h and 9a). On the other hand, due to the greatest thermally driven vertical mixing, frictional coupling of the boundary layer flow with the ground reaches a maximum in the late afternoon so an anomalous northerly wind occurs around the position of the LLJ [Blackadar, 1957; Holton, 1967; Jiang et al., 2007]. This reduces the intensity of the LLJ and northward moisture transport during the day, reducing the moisture return flow. At the same time, an anomalous southerly wind is generated above the weakened LLJ due to the northward turning of upslope flow subject to Coriolis force, which helps enhance the transport of moisture from the south into the Rocky Mountain region. In the evening, the temperature over the mountains decreases due to the shut-

down of solar insolation and the loss of heat due to longwave radiation, the east–west temperature, and associated pressure gradients then reverse direction so that the daytime ascending motion over the mountains weakens (Figures 13b and 13c). After midnight through early morning (Figures 13d and 13e), a

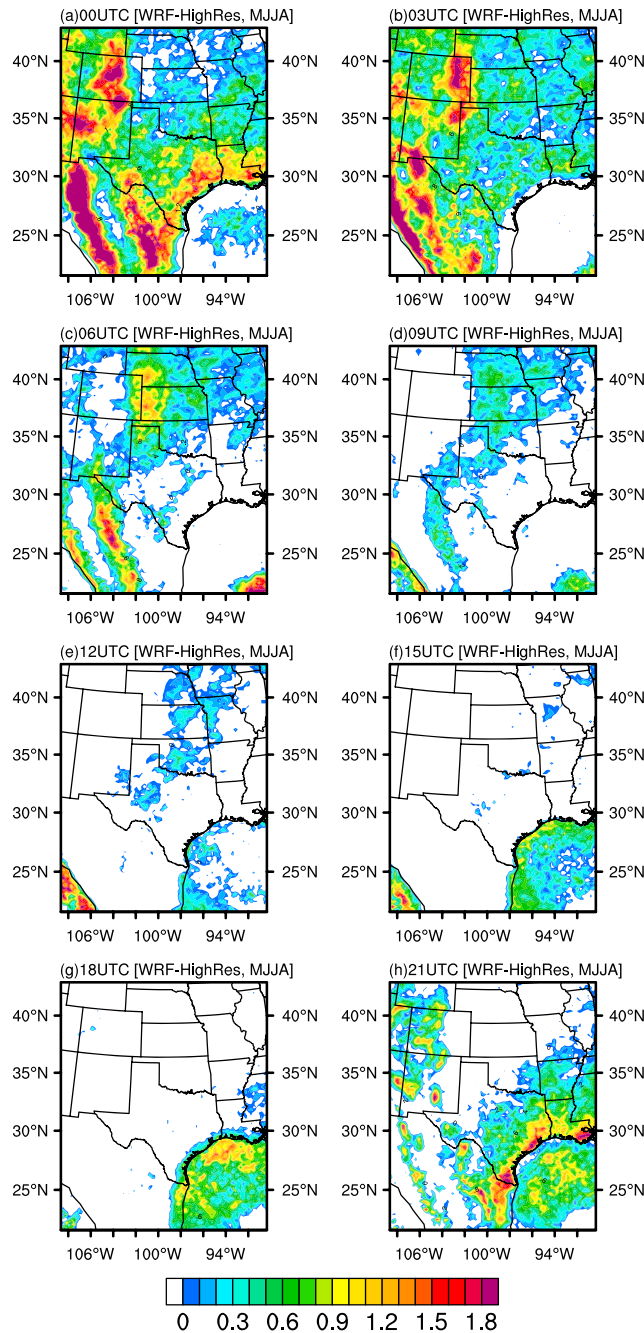


Figure 10. Same as Figure 9 but for WRF-HighRes.

nocturnal rainfall peak over the Great Plains [e.g., *Carbone et al.*, 2002; *Jiang et al.*, 2006]. To examine these behaviors in the data sets, Hovmöller diagrams of vertically averaged vertical velocity between 700 and 500 hPa and between 30°N and 40°N are presented in Figure 16. In the NARR reanalysis (Figure 14a), a clear diurnal cycle develops over the Rockies (west of 105°W). Positive vertical velocity is observed from the afternoon to early evening, and negative vertical velocity is seen overnight into the early morning. Beginning in late afternoon, the positive vertical velocity propagates eastward, reaching its maximum over the Central U.S. (between 100°W and 94°W) by 0900 UTC. The same diurnal cycle and eastward propagation signals can be seen in all the model simulations (Figures 16b and 16c). However, the anomalous vertical velocity in the WRF-HighRes simulation is greater, particularly between 105°W and 100°W (Figure 16b), consistent with the zonal circulations (Figure 14) and its anomalous precipitation signal (Figure 12c). The WRF-LowRes model

nocturnal structure of the zonal circulation is established, with a cold boundary layer over the mountains, strengthened nocturnal LLJ, ascending motion over the Great Plains, and descending motion over the Rocky Mountains. This nocturnal structure is nearly opposite to that observed in the afternoon and favors greater odds of precipitation overnight in the Plains region [*Carbone and Tuttle*, 2008]. Later into the day, the circulation transitions back to the daytime structure (Figures 13f and 13g), completing a diurnal cycle. Consistent with the eastward propagating diurnal precipitation (Figure 12c), the diurnal cycles of both solenoid circulation and LLJ are simulated reasonably well in WRF-HighRes (Figure 14), but there are obvious biases compared with those in the NARR data, specifically, the stronger vertical motion over the Rocky Mountains and weaker vertical motion over the Great Plains, and downward and eastward shift of anomaly centers for both low-level temperature and LLJ (Figure 14). Compared to the results of WRF-HighRes, WRF-LowRes produces similar but a little weaker structure of the solenoid circulation, and the LLJ anomaly is also not well represented (Figure 15).

Accompanied by the diurnal cycle of zonal circulations, convective systems propagate eastward from the Rockies to the Plains overnight. This is believed to be the primary causal factor for the observed nocturnal

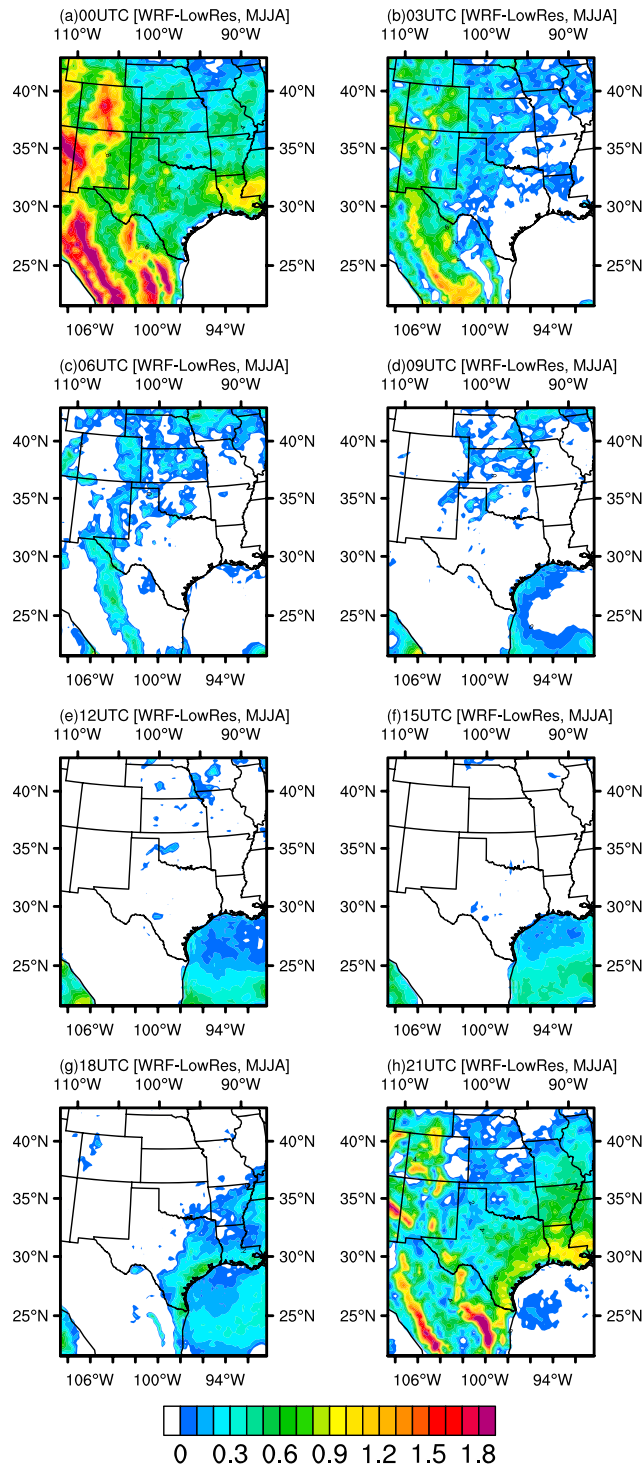


Figure 11. Same as Figure 9 but for WRF-LowRes.

6. Summary and Discussions

Dynamical downscaling of global climate model output using high-resolution regional climate models (RCMs) is now commonly used to improve coarser-resolution climate projections. Due to computational costs, so far most dynamical downscaling uses grid spacing of tens of kilometers, necessitating the use of cumulus parameterization for convective precipitation. Fortunately, computational power has been rapidly

run has a very similar diurnal cycle but a weaker intensity (Figure 16c). It should be noted that the vertical velocity in the NARR analysis is mostly model produced, and given its 32 km grid spacing, vertical velocity shown in Figure 16a is likely underestimated too.

The diurnal cycle of LLJ is further examined since it plays a critical role in the diurnal cycle of summer rainfall over the Central U.S. [e.g., Helfand and Schubert, 1995; Higgins et al., 1997; Pu and Dickinson, 2014], transporting nearly one-third of the atmospheric moisture into the continental U.S. with most of the influx occurring during the nighttime hours [Higgins et al., 1997]. Figure 17 shows the latitude-time diagram of meridional water vapor flux at 925 hPa averaged between 100°W and 95°W, showcasing the diurnal cycle of LLJ transported moisture. As shown in the NARR reanalysis (Figure 17a), the region of strong meridional moisture transport expands toward both higher and low latitudes from 0000 UTC through 0900 UTC as the LLJ intensifies, and the strong moisture transport extends northmost at around 0600 UTC or midnight local time, then it rapidly retreats to the south of 28°N by 1500 UTC and reaches another maximum around 26°N at 1200 UTC. The WRF-HighRes simulation reproduces successfully most of the aforescribed features of meridional moisture transport (Figure 17b). In WRF-LowRes (Figure 17c), the diurnal cycle of meridional moisture transport is also reasonably well simulated, but the transport magnitude is too large, and the second maximum appears to be at 0600 UTC, 3 h earlier than in WRF-HighRes and 6 h earlier than in NARR.

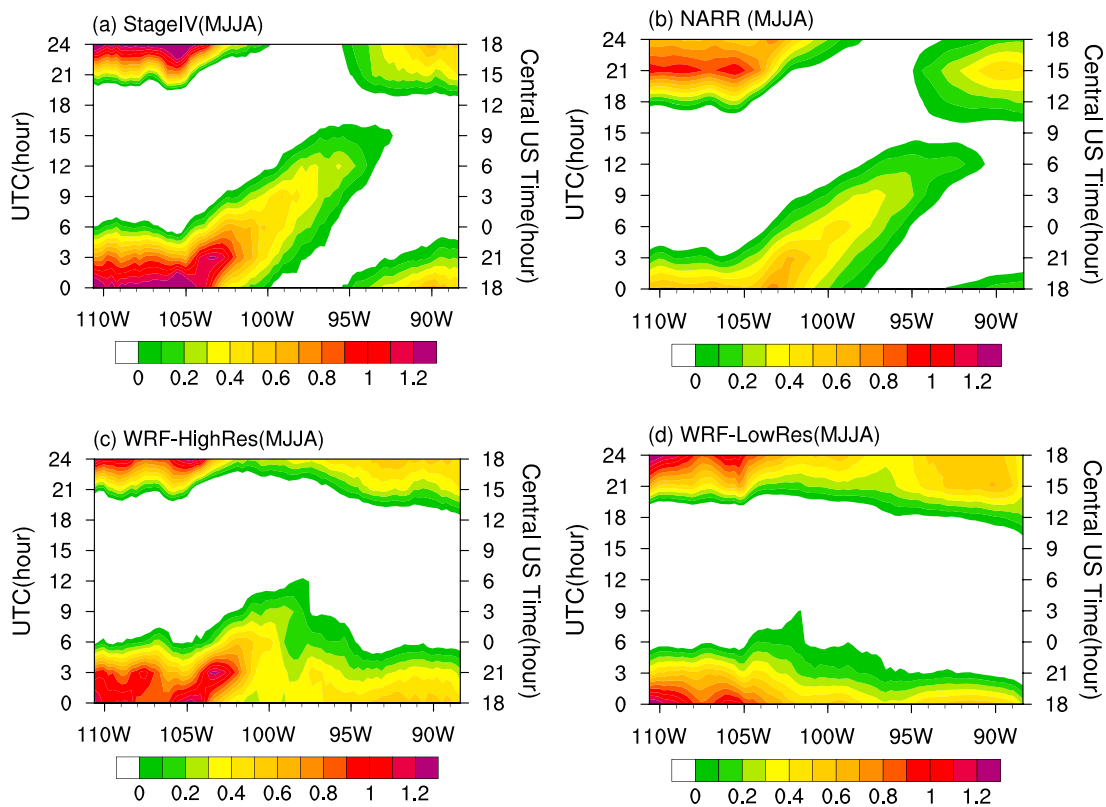


Figure 12. Hovmöller diagram of normalized diurnal precipitation deviations averaged between 30°N and 40°N of (a) Stage IV, (b) NARR, (c) WRF-HighRes, and (d) WRF-LowRes.

increasing, making RCM runs at convection-permitting/resolving resolutions feasible and allowing for explicit simulation of convection in the model. Such models have the potential to significantly improve precipitation and related water cycles as well as other mesoscale features in their simulations. They should also be able to treat topography and land surface forcing much better. The Center for Analysis and Prediction of Storms and South Central Climate Science Center at the University of Oklahoma are developing and testing an RCM based on the WRF 3.5.1 to run at a convection-permitting 4 km grid spacing for dynamical downscaling applications.

Across the U.S. central Great Plains, heavy precipitation events (above 25 mm d⁻¹) account for over half of the total MJJA rainfall. MJJA rainfall in this region is closely tied to the evolution of the nocturnal boundary layer LLJ and has a distinct diurnal cycle. Regularly initiated convection over the Rocky Mountains in the daytime often propagates eastward and reaches the Great Plains overnight. The boundary layer LLJ plays a critical role in the diurnal cycles by supplying ample moisture from the Gulf of Mexico northward into the Great Plains. It is important for RCMs to properly capture these processes.

To evaluate the WRF-based RCM for regional climate dynamical downscaling, it is run in a hindcast mode over the central U.S. covering the Great Plains and surrounding regions, at both 4 km and 25 km grid spacings, for a past 10 year period ending on 31 December 2009. The downscaling simulations are forced at the lateral boundary by the 32 km North America Regional Reanalysis (NARR) at 3-hourly intervals. Comparisons with the NARR reanalysis and Stage IV precipitation data are performed.

The results show that for a southern Great Plains verification domain, the 4 km WRF RCM is capable of reproducing some observed features of MJJA precipitation as well as the associated circulation features including the boundary layer LLJ and their diurnal variations. The 4 km WRF RCM, however, has difficulties in reproducing strong enough MJJA precipitation maximum in the Oklahoma-Kansas regions. The too-fast dissipation of the eastward propagating convective systems from the Rocky Mountains to the Plains appears to be one of the reasons. The 4 km WRF RCM does perform better than the similarly configured 25 km WRF RCM in a

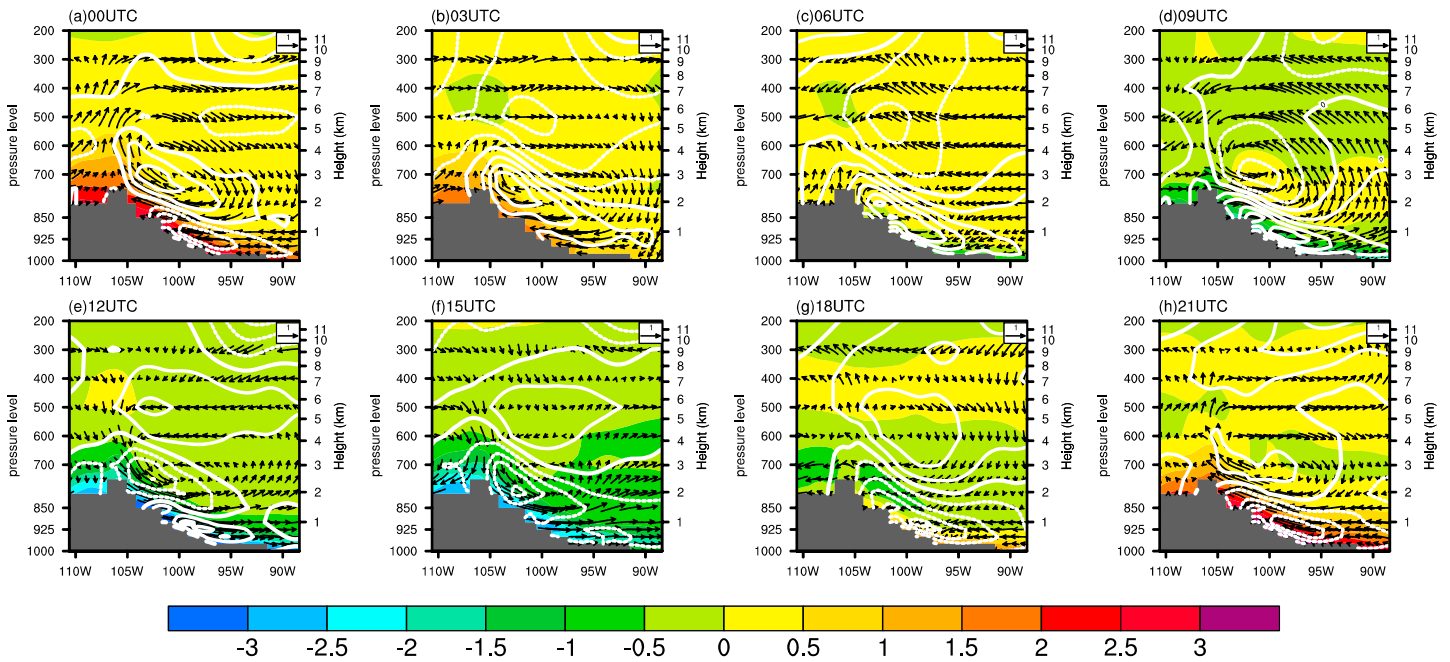


Figure 13. East-west cross sections of diurnal deviations (from daily mean) of zonal vertical circulation (u unit: m s^{-1} , w unit: cm s^{-1}), temperature (colored), and meridional wind (contours, negative values dashed) averaged between 30°N and 40°N at (a) 00:00, (b) 03:00, (c) 06:00, (d) 09:00, (e) 12:00, (f) 15:00, (g) 18:00, and (h) 21:00 UTC based on the 10 year (2000–2009) averaged NARR data.

number of areas, including pattern correlations and RMSEs compared to Stage IV in a verification domain covering Oklahoma and Kansas. The RMSEs of light and heavy rains and the 90th percentile of precipitation of the 4 km simulation are lower than those of NARR and 25 km WRF simulation, and for the total rain and the 90th percentile of precipitation, the RMSEs of 4 km WRF are about half of those of 25 km WRF, indicating better abilities of the 4 km WRF RCM in simulating the magnitude of extreme precipitation.

The 4 km WRF RCM more accurately simulates the intensity, position, and diurnal cycle of the LLJ, suggesting that the CP resolutions have more realistic model physics and dynamics important for precipitation simulations [Kopparla *et al.*, 2013; Prein *et al.*, 2013]. The results also indicate that a convection-permitting/resolving resolution has potentials for more accurately simulating the magnitude and diurnal cycle of extreme precipitation when applied to downscaling of future climate projections by general circulation models.

When viewed from most of the simulation domain, the 4 km WRF RCM still has some significant biases, including large, positive precipitation biases over the Rockies and the eastern portion of the model domain and significant low precipitation bias over the Southern Great Plains. Such biases had also been noticed in a number of previous dynamical downscaling studies over this region, although all at lower resolutions [e.g., Lee *et al.*, 2007; Mearns *et al.*, 2012; Tripathi and Dominguez, 2013]. Over-response to the orographic thermal forcing had been thought to be a reason, while associated large-scale circulation biases are also apparent. Similar biases are present in the 25 km WRF RCM, suggesting that these problems do not stem solely from the use of convective parameterization, and increasing resolution to be convection permitting does not necessarily solve the problem. Several additional 25 km sensitivity simulations performed (not shown) indicate a certain degree of sensitivity of precipitation simulation to model parameterizations, including cumulus, microphysics, and PBL schemes, but all physics configurations tested have similar overall precipitation biases. Further experimentation with model physics will still be needed, while even higher resolutions of $O(100\text{ m})$ may help reduce the biases [e.g., Bryan *et al.*, 2003; Bryan and Morrison, 2012]. With enough computational resources, it can be attempted for possibly shorter simulation periods to investigate the resolution impacts. Meanwhile, spectral nudging has been shown to be an effective way to prevent large-scale circulation biases in dynamical downscaling [Miguez-Macho *et al.*, 2004; von Storch *et al.*, 2000; Tang *et al.*, 2010; Liu *et al.*, 2012; Spero *et al.*, 2014; Wang and Kotamarthi, 2014], and it is consistent with the idea of downscaling, that is, constraining the synoptic scales to follow the driving fields while allowing the RCMs to develop small-scale

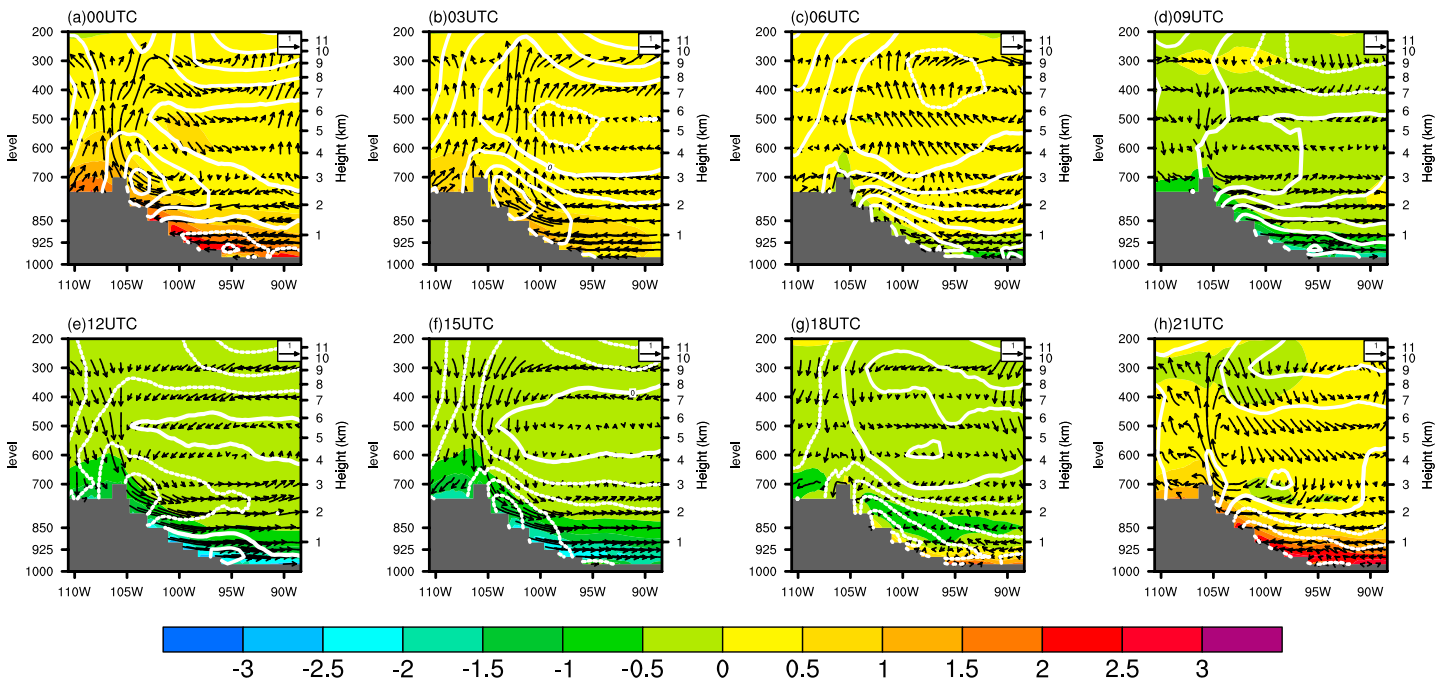


Figure 14. Same as Figure 12 but for WRF-HighRes.

dynamics. We plan to experiment with spectral nudging in our future 4 km simulations. In any case, properly simulating the magnitude, timing, and spatial distribution of convective precipitation in the historical record is critical to advancing future projections by regional climate models. Decision makers across the U.S. Great Plains, including those who are partners with the South Central Climate Science Center, are demanding these products as well as guidance toward their use for planning purposes. This study has helped to take a step forward to serve the science needs of this larger community. Determining the root causes of the precipitation

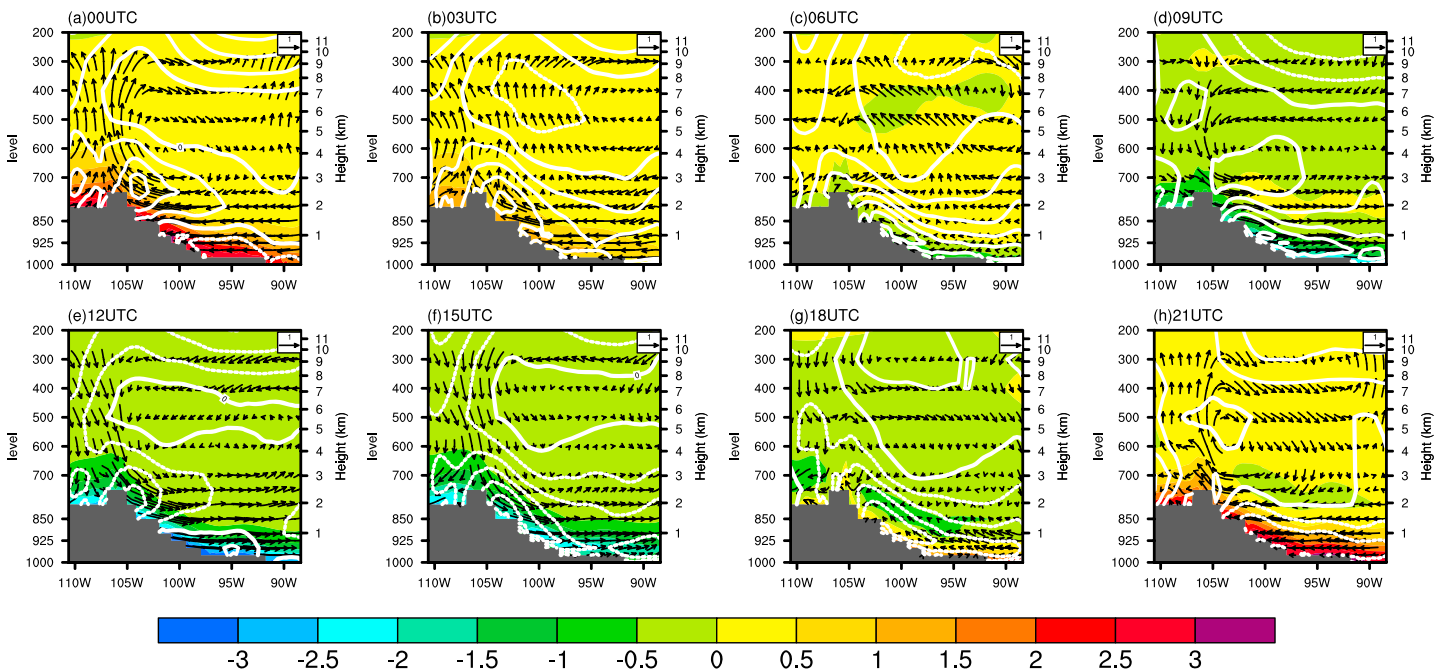


Figure 15. Same as Figure 13 but for WRF-LowRes.

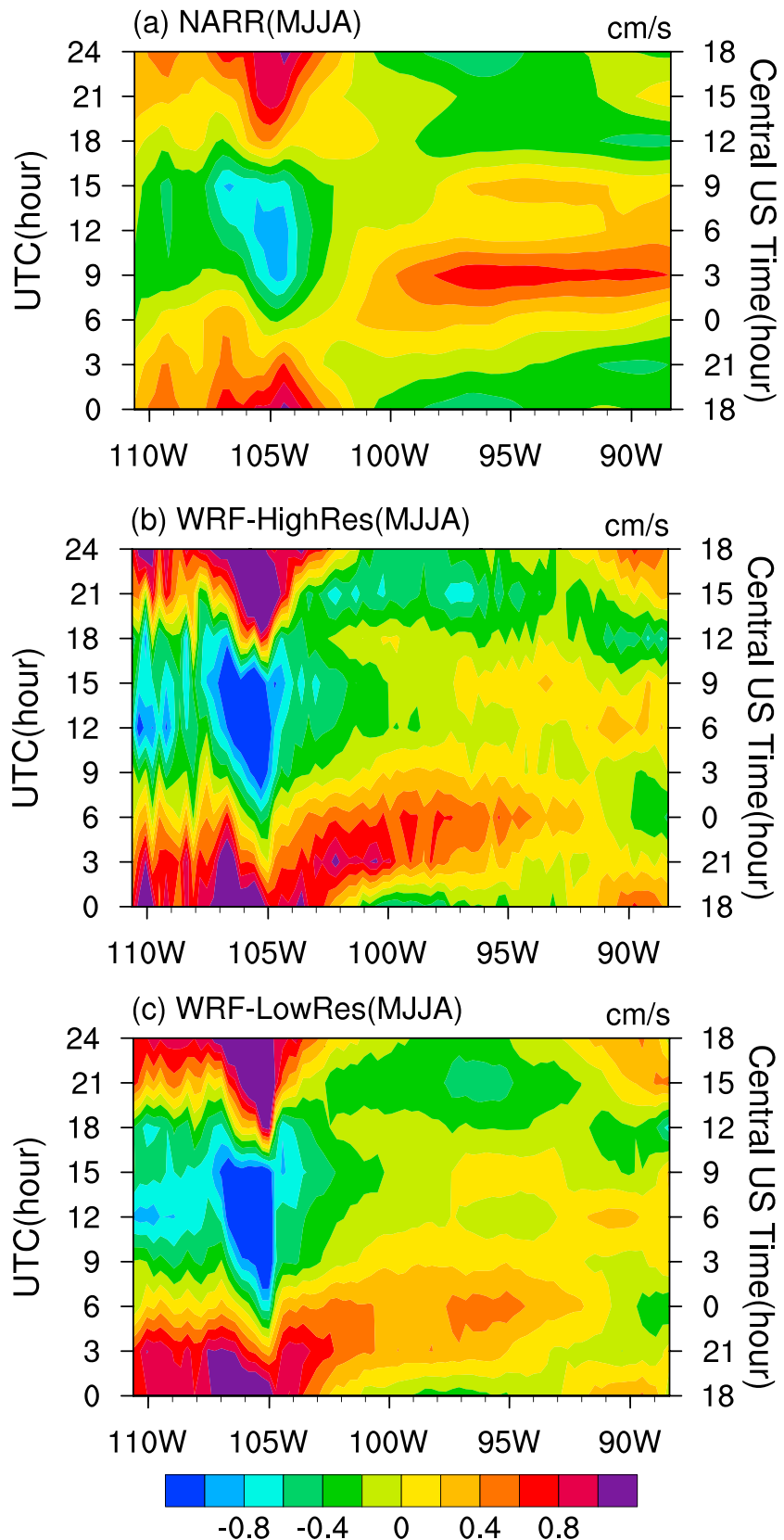


Figure 16. Similar as Figure 11 but for vertically averaged vertical velocity between 700 and 500 hPa, unit is in cm s^{-1} .

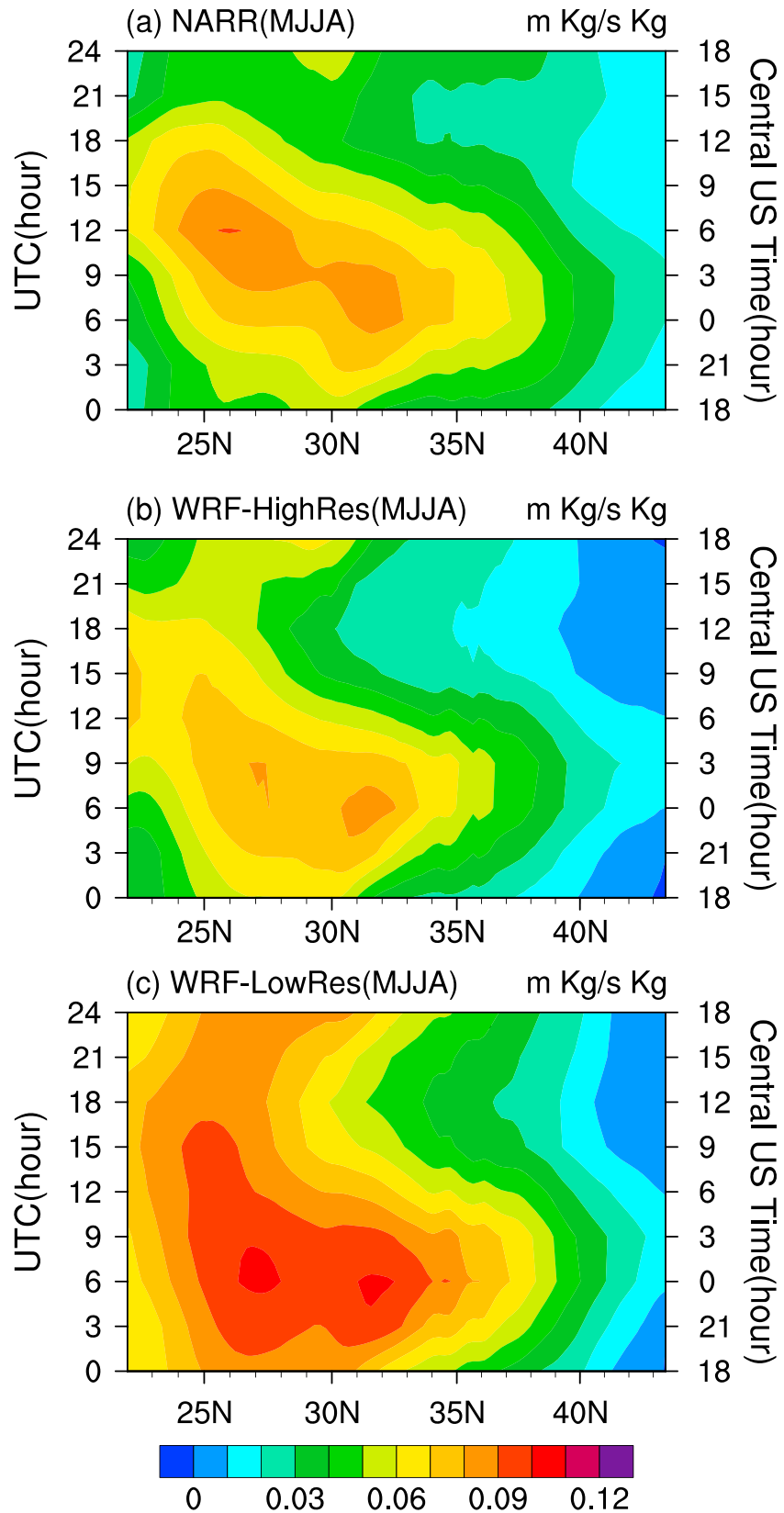


Figure 17. Latitude-time diagram of meridional water vapor flux at 925 hPa averaged between 100°W and 95°W of (a) NARR, (b) WRF-HighRes, and (c) WRF-LowRes.

biases seen in the central U.S. regions in our and earlier regional dynamic downscaling studies as well as in global climate simulations deserves careful systematic investigations.

Acknowledgments

This work was primarily supported by a grant from the U.S. Geological Survey of the U.S. Department of the Interior (grant G13AC00136) and by the University of Oklahoma Vice President of Research funding to the Center for Analysis and Prediction of Storms and the South Central Climate Science Center. The first author also thanks the support from the National Key Basic Research Program of China (grants 2010CB428504 and 2012CB417203), the National Natural Science Foundation of China (grants 41275069 and 41330420), and the CMA-NJU Joint Laboratory for Climate Prediction Studies, Institute for Climate and Global Change Research, School of Atmospheric Sciences, Nanjing University. The numerical simulations were run on an NSF Extreme Science and Engineering Discovery Environment supercomputer Stampede operated by the Texas Advanced Computing Center, and those simulation data used in this study are freely available at <http://ftp.caps.ou.edu/pub/SunJGR2016>. NARR Reanalysis data set was originally produced at NOAA's National Center for Atmospheric Prediction (NCEP) and is freely available in its original grib format through http://nomads.nccdc.noaa.gov/#narr_datasets, and Stage IV precipitation data have been archived continuously since January 2002 and freely available at <http://data.eol.ucar.edu/codiac/dss/id=21.093>. Comments and suggestions of three anonymous reviewers also significantly improved the paper.

References

- Berenguer, M., M. Surcel, I. Zawadzki, M. Xue, and F. Kong (2012), The diurnal cycle of precipitation from continental radar mosaics and numerical weather prediction models. Part II: Intercomparison among numerical models and with nowcasting, *Mon. Weather Rev.*, *140*, 2689–2705.
- Blackadar, A. K. (1957), Boundary layer wind maxima and their significance for the growth of nocturnal inversions, *Bull. Am. Meteorol. Soc.*, *38*, 283–290.
- Bonner, W. D. (1968), Climatology of the low level jet, *Mon. Weather Rev.*, *96*, 833–850.
- Borberg, F., P. Berg, P. Thejll, W. J. Gutowski, and J. H. Christensen (2010), Improved confidence in climate change projections of precipitation further evaluated using daily statistics from ENSEMBLES models, *Clim. Dyn.*, *35*, 1509–1520.
- Brockhaus, P., D. Lüthi, and C. Schär (2008), Aspects of the diurnal cycle in a regional climate model, *Meteorol. Z.*, *17*, 433–443.
- Bryan, G. H., and H. Morrison (2012), Sensitivity of a simulated squall line to horizontal resolution and parameterization of microphysics, *Mon. Weather Rev.*, *140*, 202–225.
- Bryan, G. H., J. C. Wyngaard, and J. M. Fritsch (2003), Resolution requirements for the simulation of deep moist convection, *Mon. Weather Rev.*, *131*, 2394–2416.
- Bukovsky, M. S., and D. J. Karoly (2007), A brief evaluation of precipitation from the North American Regional Reanalysis, *J. Hydrometeorol.*, *8*, 837–846.
- Bukovsky, M. S., and D. J. Karoly (2009), The sensitivity of WRF precipitation in nested regional climate simulations, *J. Appl. Meteorol. Climatol.*, *48*, 2152–2159.
- Bukovsky, M. S., and D. J. Karoly (2011), A regional modeling study of climate change impacts on warm-season precipitation in the Central United States, *J. Clim.*, *24*, 1985–2002.
- Bukovsky, M. S., D. J. Karoly, and L. O. Mearns (2013), Towards assessing NARCCAP regional climate model credibility for the North American Monsoon: Current climate simulations, *J. Clim.*, *26*, 8802–8826.
- Cai, X., Z.-L. Yang, Y. Xia, M. Huang, H. Wei, L. R. Leung, and M. B. Ek (2014), Assessment of simulated water balance from Noah, Noah-MP, CLM, and VIC over CONUS using the NLDAS test bed, *J. Geophys. Res. Atmos.*, *119*, 13,751–13,770, doi:10.1002/2014JD022113.
- Carbone, R. E., and J. D. Tuttle (2008), Rainfall occurrence in the United States warm season: The diurnal cycle, *J. Clim.*, *21*, 4132–4146.
- Carbone, R. E., J. D. Tuttle, D. A. Ahijevych, and S. B. Trier (2002), Inferences of predictability associated with warm season precipitation episodes, *J. Atmos. Sci.*, *59*, 2033–2056.
- Chen, H., T. Zhou, R. Yu, and J. Li (2009), Summer rain fall duration and its diurnal cycle over the US Great Plains, *Int. J. Climatol.*, *29*, 1515–1519.
- Clark, A. J., W. A. Gallus, and T. C. Chen (2007), Comparison of the diurnal precipitation cycle in convection-resolving and nonconvection-resolving mesoscale models, *Mon. Weather Rev.*, *135*, 3456–3473.
- Clark, A. J., W. A. Gallus Jr., M. Xue, and F. Kong (2009), A comparison of precipitation forecast skill between small convection-permitting and large convection-parameterizing ensembles, *Weather Forecasting*, *24*, 1121–1140.
- Clark, A. J., et al. (2012), An overview of the 2010 Hazardous Weather Testbed Experimental Forecast Program Spring Experiment, *Bull. Am. Meteorol. Soc.*, *93*, 55–74.
- Cook, K. H., E. K. Vizi, Z. S. Launer, and C. M. Patricola (2008), Springtime intensification of the Great Plains low-level jet and Midwest precipitation in GCM simulations of the twenty-first century, *J. Clim.*, *21*, 6321–6340.
- Dai, A., and K. E. Trenberth (2004), The diurnal cycle and its depiction in the Community Climate System Model, *J. Clim.*, *17*, 930–951.
- Dai, A., F. Giorgi, and K. E. Trenberth (1999), Observed and model simulated diurnal cycles of precipitation over the contiguous US, *J. Geophys. Res.*, *104*, 6377–6402, doi:10.1029/98JD02720.
- Demory, M.-E., P. L. Vidale, M. J. Roberts, P. Berrisford, J. Strachan, R. Schiemann, and M. S. Mizieliński (2014), The role of horizontal resolution in simulating drivers of the global hydrological cycle, *Clim. Dyn.*, *42*, 2201–2225.
- Dickinson, R., R. Errico, F. Giorgi, and G. Bates (1989), A regional climate model for the western United States, *Clim. Change*, *15*, 383–422.
- Dirmeyer, P. A., and J. L. Kinter III (2009), The Maya Express—Late spring floods in the U.S. Midwest, *Eos Trans. AGU*, *90*, 101–102.
- Dirmeyer, P. A., and K. L. Brubaker (1999), Contrasting evaporative moisture sources during the drought of 1988 and the flood of 1993, *J. Geophys. Res.*, *104*, 19,383–19,397, doi:10.1029/1999JD900222.
- Done, J., C. A. Davis, and M. Weisman (2004), The next generation of NWP: Explicit forecasts of convection using the weather research and forecasting (WRF) model, *Atmos. Sci. Lett.*, *5*, 110–117.
- Ek, M. B., K. E. Mitchell, Y. Lin, P. Grunmann, E. Rogers, G. Gayno, V. Koren, and J. D. Tarpley (2003), Implementation of the upgraded NOAA land-surface model in the NCEP operational mesoscale Eta model, *J. Geophys. Res.*, *108*(D22), 8851, doi:10.1029/2002JD003296.
- Gao, Y., J. S. Fu, J. B. Drake, Y. Liu, and J. F. Lamarque (2012), Projected changes of extreme weather events in the eastern United States based on a high resolution climate modeling system, *Environ. Res. Lett.*, *7*, 1–12.
- Garbrecht, J., and F. E. Rossel (2002), Decade-scale precipitation increase in Great Plains at end of 20th century, *J. Hydrol. Eng.*, *7*, 64–75.
- Garbrecht, J., M. Van Liew, and G. O. Brown (2004), Trends in precipitation, streamflow and evapotranspiration in the Great Plains of the United States, *J. Hydrol. Eng.*, *9*, 360–367.
- Giorgi, F., and G. T. Bates (1989), On the climatological skill of a regional model over complex terrain, *Mon. Weather Rev.*, *117*, 2325–2347.
- Grell, G. A., and S. Freitas (2013), A scale and aerosol aware stochastic convective parameterization for weather and air quality modeling, *Atmos. Chem. Phys. Discuss.*, *13*, 23,845–23,893.
- Groisman, P. Y., R. W. Knight, and T. R. Karl (2001), Heavy precipitation and high stream flow in the contiguous United States: Trends in the twentieth century, *Bull. Am. Meteorol. Soc.*, *82*, 219–246.
- Groisman, P. Y., R. W. Knight, T. R. Karl, D. R. Easterling, B. Sun, and J. H. Lawrimore (2004), Contemporary changes of the hydrological cycle over the contiguous United States: Trends derived from in situ observations, *J. Hydrometeorol.*, *5*, 64–85.
- Groisman, P. Y., R. W. Knight, D. R. Easterling, T. R. Karl, G. C. Hegerl, and V. N. Razuvaev (2005), Trends in intense precipitation in the climate record, *J. Clim.*, *18*, 1326–1350.
- Groisman, P. Y., R. W. Knight, and T. R. Karl (2012), Changes in intense precipitation over the central United States, *J. Hydrometeorol.*, *18*, 47–66.
- Helfand, H. M., and S. D. Schubert (1995), Climatology of the Great Plains low-level jet and its contribution to the continental moisture budget of the United States, *J. Clim.*, *8*, 784–806.

- Higgins, R. W., Y. Yao, E. S. Yarosh, J. E. Janowiak, and K. C. Mo (1997), Influence of the Great Plains low-level jet on summertime precipitation and moisture transport over the Central United States, *J. Clim.*, *10*, 481–507.
- Higgins, R. W., V. E. Kousky, and P. Xie (2011), Extreme precipitation events in the South-Central United States during May and June 2010: Historical perspective, role of ENSO, and trends, *J. Hydrometeorol.*, *12*, 1056–1070.
- Hohenegger, C., P. Brockhaus, and C. Schär (2008), Towards climate simulations at cloud-resolving scales, *Meteorol. Z.*, *17*, 383–394.
- Hohenegger, C., P. Brockhaus, C. S. Bretherton, and C. Schär (2009), The soil moisture-precipitation feedback in simulations with explicit and parameterized convection, *J. Clim.*, *22*, 5003–5020.
- Holton, J. R. (1967), The diurnal boundary layer wind oscillation above sloping terrain, *Tellus*, *19*, 199–205.
- Jiang, X. N., N.-C. Lau, and S. A. Klein (2006), Role of eastward propagating convection systems in the diurnal cycle and seasonal mean of summertime rainfall over the U.S. Great Plains, *Geophys. Res. Lett.*, *33*, L19809, doi:10.1029/2006GL027022.
- Jiang, X. N., N.-C. Lau, I. M. Held, and J. J. Ploshay (2007), Mechanisms of the Great Plains low-level jet as simulated in an AGCM, *J. Atmos. Sci.*, *64*, 532–547.
- Karl, T. R., and R. W. Knight (1998), Secular trends of precipitation amounts, frequency, and intensity in the United States, *Bull. Am. Meteorol. Soc.*, *79*, 231–241.
- Kong, F., et al. (2011), CAPS storm-scale ensemble forecasts in NOAA HWT 2011 Spring Experiment: Sensitivities of WRF model physics. 12th Annual WRF Users Workshop, Boulder, Colo., Paper 6.3.
- Kopparla, P., E. M. Fischer, C. Hannay, and R. Knutti (2013), Improved simulation of extreme precipitation in a high-resolution atmosphere model, *Geophys. Res. Lett.*, *40*, 5803–5808, doi:10.1002/2013GL057866.
- Kunkel, K. E., K. Andsager, and D. R. Easterling (1999), Long-term trends in extreme precipitation events over the conterminous United States and Canada, *J. Clim.*, *12*, 2515–2527.
- Lawrence, D. M., et al. (2011), Parameterization improvements and functional and structural advances in version 4 of the Community Land Model, *J. Adv. Model. Earth Syst.*, *3*, M03001, doi:10.1029/2011MS000045.
- Lee, M.-I., et al. (2007), Sensitivity to horizontal resolution in the AGCM simulations of warm season diurnal cycle of precipitation over the United States and Northern Mexico, *J. Clim.*, *20*, 1862–1881.
- Leung, L. R., Y. Qian, X. Bian, W. M. Washington, J. Han, and J. O. Roads (2004), Mid-century ensemble regional climate change scenarios for the western United States, *Clim. Change*, *62*, 75–113.
- Lin, X., D. A. Randall, and L. D. Fowler (2000), Diurnal variability of the hydrologic cycle and radiative fluxes: Comparisons between observations and a GCM, *J. Clim.*, *13*, 4159–4179.
- Lin, Y., and K. E. Mitchell (2005), The NCEP Stage II/IV hourly precipitation analyses: Development and applications. Preprints, 19th Conf. on Hydrology, Am. Meteorol. Soc., San Diego, Calif., 9–13 January 2005, Paper 1.2.
- Liu, P., A. P. Tsimpidi, Y. Hu, B. Stone, A. G. Russell, and A. Nenes (2012), Differences between downscaling with spectral and grid nudging using WRF, *Atmos. Chem. Phys.*, *12*(8), 3601–3610, doi:10.5194/acp-12-3601-2012.
- Maddox, R. A., C. F. Chappell, and L. R. Hoxit (1979), Synoptic and meso-scale aspects of flash flood events, *Bull. Am. Meteorol. Soc.*, *60*, 115–123.
- Mahoney, K., M. Alexander, J. D. Scott, and J. Barsugli (2013), High-resolution downscaled simulations of warm-season extreme precipitation events in the Colorado Front Range under past and future climates, *J. Clim.*, *26*, 8671–8689.
- Mass, C., D. Ovens, M. Albright, and K. Westrick (2002), Does increasing horizontal resolution produce better forecasts? The results of two years of real-time numerical weather prediction in the Pacific Northwest, *Bull. Am. Meteorol. Soc.*, *83*, 407–430.
- Means, L. L. (1956), Some basic parameters associated with the flood rains at Chicago, October 9–12, 1954, *Mon. Weather Rev.*, *84*, 253–260.
- Mearns, L. O., W. J. Gutowski, R. Jones, L.-Y. Leung, S. McGinnis, A. M. B. Nunes, and Y. Qian (2009), A regional climate change assessment program for North America, *Eos Trans. AGU*, *90*, 311, doi:10.1029/2009EO360002.
- Mearns, L. O., et al. (2012), The North American Regional Climate Change Assessment Program: Overview of phase I results, *Bull. Am. Meteorol. Soc.*, *93*, 1337–1362.
- Mesinger, F., et al. (2006), North American Regional Reanalysis, *Bull. Am. Meteorol. Soc.*, *87*, 343–360.
- Miguez-Macho, G., G. L. Stenchikov, and A. Robock (2004), Spectral nudging to eliminate the effects of domain position and geometry in regional climate model simulations, *J. Geophys. Res.*, *109*, D13104, doi:10.1029/2003JD004495.
- Mo, K. C., M. Chelliah, M. Carrera, R. W. Higgins, and W. Ebisuzaki (2005), Atmospheric moisture transport over the United States and Mexico as evaluated from the NCEP Regional Reanalysis, *J. Hydrometeorol.*, *6*, 710–728.
- Molinari, J., and M. Dudek (1992), Parameterization of convective precipitation in mesoscale numerical models: A critical review, *Mon. Weather Rev.*, *120*, 326–344.
- Moore, B. J., P. J. Neiman, F. M. Ralph, and F. E. Barthold (2012), Physical processes associated with heavy flooding rainfall in Nashville, Tennessee, and Vicinity during 1–2 May 2010: The role of an atmosphere river and mesoscale convective systems, *Mon. Weather Rev.*, *140*, 358–378.
- Oleson, K. W., et al. (2010), Technical description of version 4.0 of the Community Land Model (CLM), *NCAR Tech. Note NCAR/TN-478 + STR*, 257 pp., Natl. Cent. for Atmos. Res., Boulder, Colo.
- Pan, L.-L., S.-H. Chen, D. Cayan, M.-Y. Lin, Q. Hart, M.-H. Zhang, Y. Liu, and J. Wang (2011), Influences of climate change on California and Nevada regions revealed by a high-resolution dynamical downscaling study, *Clim. Dyn.*, *37*, 2005–2020.
- Pope, V. D., and R. A. Stratton (2002), The processes governing horizontal resolution sensitivity in climate models, *Clim. Dyn.*, *19*, 211–236.
- Prat, O. P., and B. R. Nelson (2015), Evaluation of precipitation estimates over CONUS derived from satellite, radar, and rain gauge data sets at daily to annual scales (2002–2012), *Hydrol. Earth Syst. Sci.*, *19*, 2037–2056.
- Prein, A. F., A. Gobiet, M. Suklitsch, H. Truhetz, N. K. Awan, K. Keuler, and G. Georgievski (2013), Added value of convection permitting seasonal simulations, *Clim. Dyn.*, *41*, 2655–2677.
- Pu, B., and R. E. Dickinson (2014), Diurnal spatial variability of Great Plains summer precipitation related to the dynamics of the low-level jet, *J. Atmos. Sci.*, *71*, 1807–1817.
- Qian, Y., W. I. Gustafson Jr., and J. D. Fast (2010), An investigation of the sub-grid variability of trace gases and aerosols for global climate models, *Atmos. Chem. Phys.*, *10*, 6917–6946.
- Rasmusson, E. M. (1967), Atmospheric water vapor transport and the water balance of North America. Part I: Characteristics of the water vapor flux field, *Mon. Weather Rev.*, *95*, 403–426.
- Rauscher, S., E. Coppola, C. Piani, and F. Giorgi (2010), Resolution effects on regional climate model simulations of seasonal precipitation over Europe, *Clim. Dyn.*, *35*, 685–711.
- Roberts, N. M., and H. W. Lean (2008), Scale-selective verification of rainfall accumulations from high-resolution forecasts of convective events, *Mon. Weather Rev.*, *136*, 78–97.

- Roeckner, E., R. Brokopf, M. Esch, M. Giorgetta, S. Hagemann, L. Kornblueh, E. Manzini, U. Schlese, and U. Schulzweida (2006), Sensitivity of simulated climate to horizontal and vertical resolution in the ECHAM5 atmosphere model, *J. Clim.*, *19*, 3771–3791.
- Ruiz-Barradas, A., and S. Nigam (2005), Warm-season rainfall variability over the US Great Plains in observations, NCEP and ERA-40 Reanalyses, and NCAR and NASA atmospheric model simulations, *J. Clim.*, *18*, 1808–1829.
- Ruiz-Barradas, A., and S. Nigam (2006), Great Plains hydroclimate variability: The view from North American Regional Reanalysis, *J. Clim.*, *19*, 3004–3010.
- Salathé, E. P., R. Steed, C. F. Mass, and P. Zahn (2008), A high-resolution climate model for the U.S. Pacific Northwest: Mesoscale feedbacks and local responses to climate change, *J. Clim.*, *21*, 5708–5726.
- Schwartz, C. S., J. S. Kain, S. J. Weiss, M. Xue, D. R. Bright, F. Kong, K. W. Thomas, J. J. Levit, M. C. Coniglio, and M. S. Wandishin (2010), Toward improved convection-allowing ensembles: Model physics sensitivities and optimizing probabilistic guidance with small ensemble membership, *Weather Forecasting*, *25*, 263–280.
- Schwartz, C., J. Kain, S. Weiss, M. Xue, D. Bright, F. Kong, K. Thomas, J. Levit, and M. Coniglio (2009), Next-day convection-allowing WRF model guidance: A second look at 2 vs. 4 km grid spacing, *Mon. Weather Rev.*, *137*, 3351–3372.
- Shaffrey, L. C., et al. (2009), U.K. HiGEM: The new U.K. High-Resolution Global Environment Model—Model description and basic evaluation, *J. Clim.*, *22*, 1861–1896.
- Skamarock, W. C., J. B. Klemp, J. Dudhia, D. O. Gill, D. M. Barker, W. Wang, and J. G. Powers (2005), A description of the Advanced Research WRF version 2., *NCAR Tech. Note NCAR/TN-468 + STR*, 88 pp, Natl. Cent. for Atmos. Res., Boulder, Colo.
- Skamarock, W. C., J. B. Klemp, J. Dudhia, D. O. Gill, D. M. Barker, M. G. Duda, X.-Y. Huang, W. Wang, and J. G. Powers (2008), A description of the Advanced Research WRF version 3., *NCAR Tech. Note NCAR/TN-475 + STR*, 113 pp, Natl. Cent. for Atmos. Res., Boulder, Colo.
- Spero, T. L., M. J. Otte, J. H. Bowden, and C. G. Nolte (2014), Improving the representation of clouds, radiation, and precipitation using spectral nudging in the Weather Research and Forecasting model, *J. Geophys. Res. Atmos.*, *119*, 11,682–11,694, doi:10.1002/2014jd022173.
- Surcel, M., M. Berenguer, and I. Zawadzki (2010), The diurnal cycle of precipitation from continental radar mosaics and numerical weather prediction models. Part I: Methodology and seasonal comparison, *Mon. Weather Rev.*, *138*, 3084–3106.
- Tang, J., S. Song, and J. Wu (2010), Impacts of the spectral nudging technique on simulation of the East Asian summer monsoon, *Theor. Appl. Climatol.*, *101*, 41–51.
- Trapp, R. J., E. D. Robinson, M. E. Baldwin, N. S. Diffsenbaugh, and B. R. J. Schwedler (2011), Regional climate of hazardous convective weather through high-resolution dynamical downscaling, *Clim. Dyn.*, *37*, 677–689.
- Trenberth, K. E., A. Dai, R. M. Rasmussen, and D. B. Parsons (2003), The changing character of precipitation, *Bull. Am. Meteorol. Soc.*, *84*, 1205–1217.
- Tripathi, O. P., and F. Dominguez (2013), Effects of spatial resolution in the simulation of daily and subdaily precipitation in the southwestern US, *J. Geophys. Res. Atmos.*, *118*, 7591–7605, doi:10.1002/jgrd.50590.
- Villarini, G., E. Scoccimarro, and S. Gualdi (2013), Projections of heavy rainfall over the central United States based on CMIP5 models, *Atmos. Sci. Lett.*, *14*, 200–205.
- von Storch, H., H. Langenberg, and F. Feser (2000), A spectral nudging technique for dynamical downscaling purposes, *Mon. Weather Rev.*, *128*(10), 3664–3673, doi:10.1175/1520-0493(2000)128<3664:Asntfd>2.0.Co;2.
- Wallace, J. M. (1975), Diurnal variations in precipitation and thunderstorm frequency over the conterminous United States, *Mon. Weather Rev.*, *103*, 406–419.
- Wang, J., and V. R. Kotamarthi (2014), Downscaling with a nested regional climate model in near-surface fields over the contiguous United States, *J. Geophys. Res. Atmos.*, *119*, 8778–8797, doi:10.1002/2014JD021696.
- Weaver, S. J., and S. Nigam (2008), Variability of the Great Plains low-level jet: Large-scale circulation context and hydroclimate impacts, *J. Clim.*, *21*, 1532–1551.
- Weisman, M. L., W. C. Skamarock, and J. B. Klemp (1997), The resolution dependence of explicitly modeled convective systems, *Mon. Weather Rev.*, *125*, 527–548.
- Weisman, M. L., C. Davis, W. Wang, K. W. Manning, and J. B. Klemp (2008), Experiences with 0–36-h explicit convective forecasts with the WRF-ARW model, *Weather Forecasting*, *23*, 407–437.
- Xue, M., et al. (2007), CAPS realtime storm-scale ensemble and high-resolution forecasts as part of the NOAA hazardous weather testbed 2007 spring experiment. 22nd Conf. Wea. Anal. Forecasting/18th Conf. Num. Wea. Pred., Salt Lake City, Utah, *Am. Meteorol. Soc.*, CDROM 3B.1.
- Xue, M., et al. (2008), CAPS realtime storm-scale ensemble and high-resolution forecasts as part of the NOAA Hazardous Weather Testbed 2008 Spring Experiment, 24th Conf. Several Local Storms, Savannah, Ga, *Am. Meteorol. Soc.*, 12.2 pp.
- Xue, M., et al. (2009), CAPS realtime multi-model convection-allowing ensemble and 1-km convection-resolving forecasts for the NOAA Hazardous Weather Testbed 2009 Spring Experiment. 23rd Conf. Wea. Anal. Forecasting/19th Conf. Num. Wea. Pred., Omaha, Nebr., *Am. Meteorol. Soc.*, Paper 16.
- Xue, M., et al. (2011), CAPS realtime storm scale ensemble and high resolution forecasts for the NOAA Hazardous Weather Testbed 2010 Spring Experiment, 24th Conf. Wea. Forecasting/20th Conf. Num. Wea. Pred., *Am. Meteorol. Soc.*, Paper 9A.2.
- Xue, M., F. Kong, K. W. Thomas, J. Gao, Y. Wang, K. A. Brewster, and K. K. Droegemeier (2013), Prediction of convective storms at convection-resolving 1 km resolution over continental United States with radar data assimilation: An example case of 26 May 2008 and precipitation forecasts from spring 2009, *Adv. Meteorol.*, *2013*, 259052.